

# Hierarchical Black-Hole Mergers in Multiple Systems: Constrain the Formation of GW190412, GW190814 and GW190521-like events

Bin Liu<sup>1</sup>, Dong Lai<sup>1,2</sup>

<sup>1</sup> *Cornell Center for Astrophysics and Planetary Science, Department of Astronomy, Cornell University, Ithaca, NY 14853, USA*

<sup>2</sup> *Tsung-Dao Lee Institute, Shanghai Jiao Tong University, Shanghai 200240, China*

24 October 2021

## ABSTRACT

The merging black-hole (BH) binaries GW190412, GW190814 and GW190521 from the third LIGO/VIRGO observing run exhibit some extraordinary properties, including highly asymmetric masses, significant spin, and component mass in the “mass gap”. These features can be explained if one or both components of the binary are the remnants of previous mergers. In this paper, we explore hierarchical mergers in multiple stellar systems, taking into account the natal kick and mass loss due to the supernova explosion (SN) on each component, as well as the merger kick received by the merger remnant. The binaries that have survived the SNe and kicks generally have too wide orbital separations to merge by themselves, but can merge with the aid of an external companion that gives rise to Lidov-Kozai oscillations. The BH binaries that consist of second-generation BHs can also be assembled in dense star clusters through binary interactions. We characterize the parameter space of these BH binaries by merger fractions in an analytical approach. Combining the distributions of the survived binaries, we further constrain the parameters of the external companion, using the analytically formulated tertiary perturbation strength. We find that to produce the three LIGO/VIRGO O3 events, the external companions must be at least a few hundreds  $M_{\odot}$ , and fall in the intermediate-mass BH and supermassive BH range. We suggest that GW190412, GW190814 and GW190521 could all be produced via hierarchical mergers in multiples, likely in a nuclear star cluster, with the final merger induced by a massive BH.

**Key words:** binaries: general - black hole physics - gravitational waves - stars: black holes - stars: kinematics and dynamics

## 1 INTRODUCTION

The detections of gravitational waves from merging binary black holes (BHs) (e.g., Abbott et al. 2019a,b) have motivated many recent studies on their formation channels, including the traditional isolated binary evolution (e.g., Lipunov et al. 1997, 2017; Podsiadlowski et al. 2003; Belczynski et al. 2010, 2016; Dominik et al. 2012, 2013, 2015), the chemically homogeneous evolution (e.g., Mandel & de Mink 2016; Marchant et al. 2016), the gas-assisted mergers in AGN disks (e.g., Bartos et al. 2017), and various flavors of dynamical channels that involve either strong gravitational scatterings in dense clusters (e.g., Portegies Zwart &

McMillan 2000; O’Leary et al. 2006; Miller & Lauburg 2009; Banerjee et al. 2010; Downing et al. 2010; Ziosi et al. 2014; Rodriguez et al. 2015; Samsing & D’Orazio 2018) or Lidov-Kozai induced mergers in isolated triple and quadruple systems (e.g., Blaes et al. 2002; Miller & Hamilton 2002; Wen 2003; Antonini & Perets 2012; Antonini et al. 2017; Silsbee & Tremaine 2017; Hoang et al. 2018; Liu & Lai 2018, 2019, 2020; Randall & Xianyu 2018; Liu et al. 2019a,b; Fragione & Kocsis 2019a; Fragione & Loeb 2019b).

The BH mergers detected in the first and second runs (O1 and O2) of LIGO/VIRGO typically feature binaries with comparable masses (i.e.,  $m_2/m_1 \sim 0.6 - 0.9$ ) and

mass-weighted effective spin parameter  $\chi_{\text{eff}}$  consistent with  $\chi_{\text{eff}} \sim 0$  (but see [Zackay et al. 2019](#); [Venumadhav et al. 2020](#)). However, the recent detections in the third observing run (O3) of LIGO/VIRGO reveal the existence of different types of black hole binaries (BHBs). In GW190412 ([Abbott et al. 2020a](#)), the BHB has component masses  $29.7^{+5.0}_{-5.3} M_{\odot}$  and  $8.4^{+1.7}_{-1.0} M_{\odot}$ . The primary (more massive) BH is inferred to rotate rapidly, with the dimensionless spin (Kerr) parameter  $\chi_1 = 0.43^{+0.16}_{-0.26}$ . The effective spin parameter of the BHB is constrained to be  $\chi_{\text{eff}} = 0.25^{+0.09}_{-0.11}$ , indicating a non-negligible spin-orbit misalignment angle. In the second event GW190814 ([Abbott et al. 2020c](#)), the merging binary involves a  $23.2^{+1.1}_{-1.0} M_{\odot}$  BH and a compact object with mass  $2.6^{+0.08}_{-0.09} M_{\odot}$  in the so-called low mass gap of  $(2M_{\odot} - 5M_{\odot})$  (e.g., [Bailyn et al. 1998](#); [Özel et al. 2010](#); [Farr et al. 2011](#)); the secondary could be a heavy neutron star (NS) or a light BH. In this source, the primary spin is tightly constrained to a small value ( $\chi_1 \lesssim 0.07$ ), while the secondary spin is unconstrained. In GW190521 ([Abbott et al. 2020d](#)), the two BHs have masses of  $85^{+21}_{-14} M_{\odot}$  and  $66^{+17}_{-18} M_{\odot}$ , both of which may fall in the high mass gap produced by the (pulsational) pair-instability supernova processes ( $65M_{\odot} - 120M_{\odot}$ ) (e.g., [Barkat et al. 1967](#); [Woosley 2017](#)). The analyses of GW190521 indicate that the two BHs are fast-rotating with  $\chi_1 = 0.69^{+0.27}_{-0.62}$  and  $\chi_2 = 0.73^{+0.24}_{-0.64}$ , while the binary has an effective spin  $\chi_{\text{eff}} = 0.08^{+0.27}_{-0.36}$  and “perpendicular” spin  $\chi_p = 0.68^{+0.25}_{-0.37}$ , again suggesting significant spin-orbit misalignments.

The astrophysical origin of these three LIGO events are still under debate. The mergers of BHBs with extreme mass ratios (as in GW190412 and GW190814) or component masses in the mass gap (as in GW190521) are expected to be rather uncommon, especially if the merging binary contains two first generation (1G) BHs (e.g., [Gerosa et al. 2020](#)). Indeed, recent studies suggest that GW190412-and/or GW190814-like events should be rare in many formation models, including isolated binaries with tidally spun-up secondaries (e.g., [Olejak et al. 2020](#); [Mandel & Fragos 2020](#)), dynamical assembly in dense star clusters (e.g., [Di Carlo et al. 2020](#); [Rodriguez et al. 2020](#); [Zevin et al. 2020](#); [Samsing & Hotokezaka 2020](#)), gas-assisted formation in AGN disks (e.g., [Yang et al. 2020](#)), as well as the triple/quadruple stars (e.g., [Hamers & Safarzadeh 2020](#); [Lu et al. 2021](#)).

The unexpected features of these three O3 events may be naturally explained if one or both components are the remnants of the previous BH or NS mergers. This is generally termed “hierarchical mergers” (e.g., [Abbott et al. 2020e](#)), but exactly how successive mergers occur and with what frequencies are not clear. In this paper, we study hierarchical mergers involving binaries and multiples, where the multiples could be either “primordial” or formed dynamically in dense stellar clusters (see Figures 1-3). In particular, we consider the  $(30M_{\odot})$  primary in GW190412 to be a merger product — this would explain its large observed spin. We suggest the secondary ( $2.6M_{\odot}$ ) in GW190814 to be produced by the merger of two canonical ( $1.3 - 1.4M_{\odot}$ ) NSs. We

## Formation of GW190412-like binaries

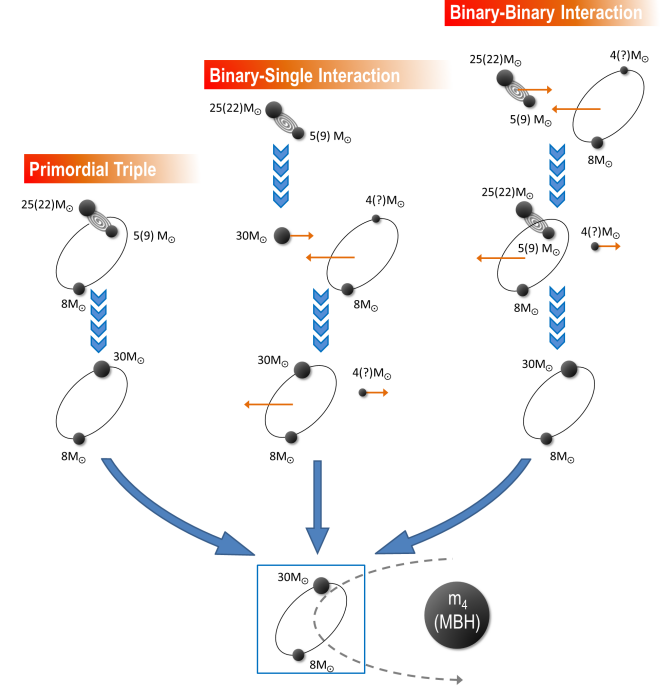


**Figure 1.** Different formation pathways of GW190412-like systems. The final merging BHB can be produced either in a primordial multiple system (left), or through binary-single interaction (middle) and binary-binary interaction (right). The final BHB is unlikely to merge by itself, but can be induced to merge by an external body (likely a massive BH). We label the possible values of the individual masses based on the analysis in Section 3 (see also Section 6). Two possible sets of the binary progenitor masses are given for the  $30M_{\odot}$  BH. The number with a question mark implies that the mass is not well constrained.

assume both massive components in GW190521 to be the products of first-generation mergers — this would explain their large observed spins. Regardless of the detailed evolutionary pathways, it is likely the final BHBs cannot merge by themselves because of their wide orbital separations. Instead, they undergo mergers induced by a tertiary companion, likely a massive or supermassive BH (MBH, SMBH), through the Lidov-Kozai mechanism (e.g., [Lidov 1962](#); [Kozai 1962](#)). Overall, we envision that through different pathways (Figures 1-3), a final BHB is assembled, likely in a dense nuclear star cluster, and the final merger is induced by a MBH or SMBH. We examine the possibility and constraints that systems like GW190412, GW190814 and GW190521 are produced in multiple systems.

A specific scenario for the formation of merging BHBs relies on “primordial” triples or quadruples (the leftmost pathway in Figures 1-3). We study this “primordial” multiple scenario in details for each of the three LIGO/VIRGO O3 systems. Figure 4 illustrates the key physical processes, using GW190412 as an example. We consider a hierarchical quadruple system, consisting of three nested binaries. The innermost binary has masses  $m_1$ ,  $m_2$ , and moves around  $m_3$

## Formation of GW190814-like binaries

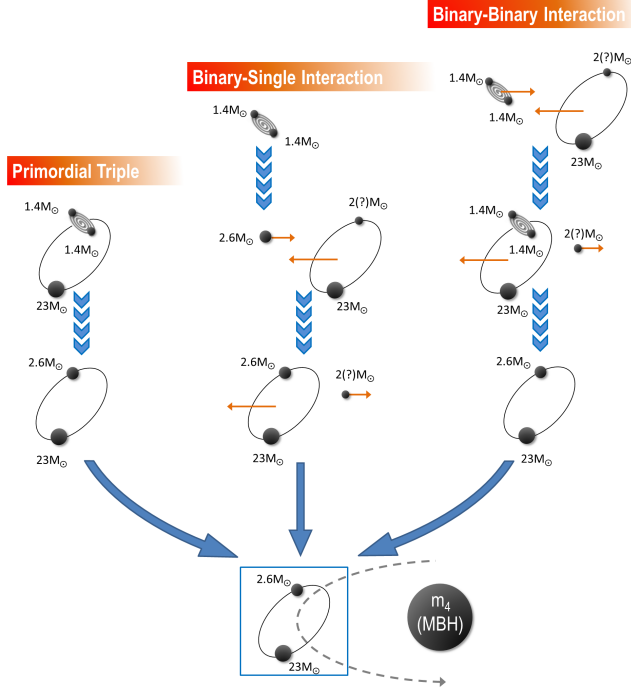


**Figure 2.** Similar to Figure 1, but for GW190814-like systems (see Sections 4 and 6).

forming the middle binary. This triple system also orbits around the fourth body with mass  $m_4$ , constituting the outer binary. While  $m_1, m_2, m_3$  have “stellar” masses ( $\sim 1M_\odot$  to tens of  $M_\odot$ ), we consider a wide range of possible  $m_4$ , from stellar mass BH to SMBH. To produce GW190412, each star in the inner triple undergoes stellar evolution and eventually collapses into a BH, possibly accompanied by a natal kick and sudden mass loss during the supernova (SN) explosion. The innermost BHB is assumed to merge by itself, as in the standard isolated binary evolution channel, and the merger remnant receives a merger kick, with the kick magnitude depending on the mass ratio. Under appropriate conditions (e.g. the kick velocity is not too high), this newly formed BH ( $m_{12}$ ) may remain bound to  $m_3$  in the “middle” binary to constitute a triple system together with  $m_4$  (see Figure 4). We envision that, with the aid of tertiary companion ( $m_4$ ), the middle binary may merge eventually via Lidov-Kozai (LK) oscillations when the mutual inclination between the middle and outer binaries is sufficiently high. A similar process applies to GW190814, where the secondary component comes from the merger of two NSs in the innermost binary. For GW190521, we consider a quadruple system orbiting around an external companion ( $m_5$ ), where two binaries in the quadruple merge individually, leaving behind a BHB and the tertiary ( $m_5$ ).

Most previous works on BH binary mergers in multiple systems consider specific numerical examples or carry out some kinds of “population synthesis” (i.e., Liu & Lai 2018; Liu et al. 2019a; Fragione & Kocsis 2019a; Hamers & Sa-

## Formation of GW190521-like binaries

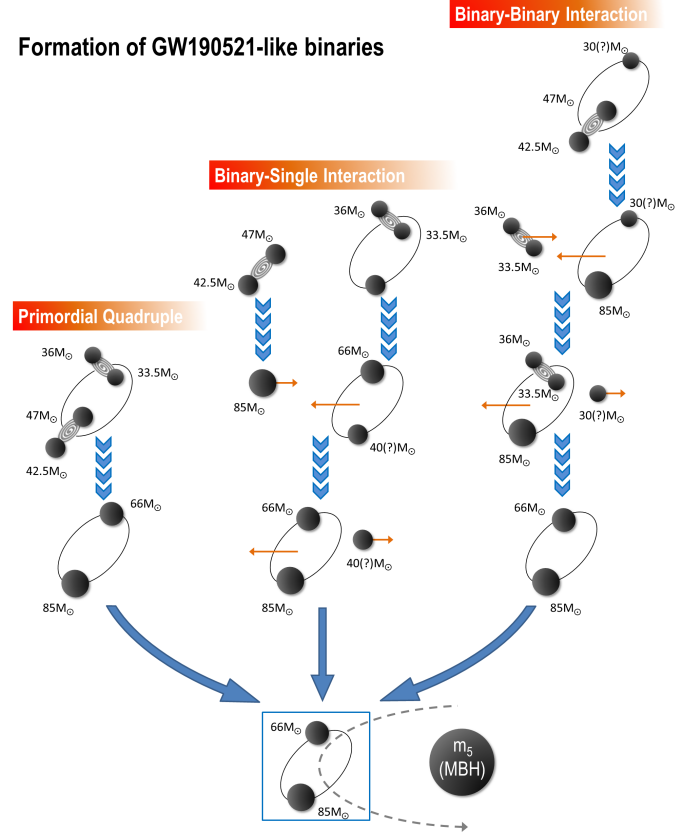


**Figure 3.** Similar to Figure 1, but for GW190521-like systems (see Sections 5 and 6). Other possible dynamical pathways involving single-triple interaction and binary-triple interaction are not shown.

farzadeh 2020) with various assumptions about the progenitor populations. However, using the results from Liu & Lai (2018), all essential aspects of the leading-order LK-induced mergers, including the merger “window” and merger fraction, can be understood analytically. We summarize and extend these analytical results (including new fitting formulae) in this paper (see Section 2.2). This allows us to constrain the property of the outer binary ( $m_4$  or  $m_5$  and the semi-major axis  $a_{\text{out}}$ ) without performing extensive population calculations.

Our paper is organized as follows. In Section 2, we present the key physical ingredients for studying BHB mergers in multiple systems. Section 2.1 describes the effects of natal kicks (associated with NS and BH formation in a SN explosion) and merger kicks on hierarchical systems; these are relevant for the “primordial” multiple scenario of Figures 1-3. In Section 2.2, we derive the general analytical expressions for the merger fraction and perturbation strength in tertiary-induced mergers of BHBs; these are relevant for both “primordial” multiple and “dynamical” multiple scenarios of Figures 1-3. In Section 3, we explore the formation of GW190412 in the “primordial” multiple scenario, where the system experiences natal kicks and mergers in sequence. Based on the distributions of post-kick orbital parameters

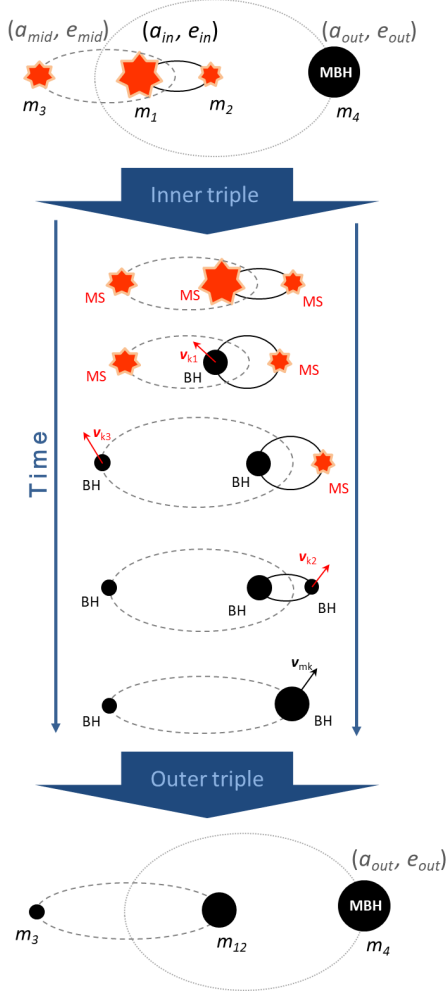


**Figure 4.** Detailed evolutionary diagram of a hierarchical quadruple system leading to the formation of GW190412-like systems. This corresponds to the “primordial” pathway depicted in Figure 1. We consider three nested binaries, where the component masses are  $m_1$ ,  $m_2$ ,  $m_3$  and  $m_4$  (e.g., the inner triple could reside in a nuclear star cluster surrounding a massive BH  $m_4$ ). The semi-major axes and eccentricities are denoted by  $a_{\text{in}}$ ,  $a_{\text{mid}}$ ,  $a_{\text{out}}$  and  $e_{\text{in}}$ ,  $e_{\text{mid}}$ ,  $e_{\text{out}}$ , respectively. The inner triple stars undergo SN explosions accompanied by natal kicks and mass losses. The merger of the inner binary is accompanied by a merger kick due to asymmetric GW emission. If the middle binary survives all the SNs and kicks, it continues the “final” BHB and can merge due to LK oscillations with the aid of an external body  $m_4$  (a massive or supermassive BH).

of the “final” BHBs, we constrain the parameter space of the external perturber (the MBH) required to effectively induce mergers of the BHBs. In Sections 4 and 5, we examine the formation of GW190814 and GW190521, respectively, using the similar approach. In Section 6, we consider the dynamical formation pathways of the final BHBs (involving single-binary and binary-binary scatterings; see Figures 1-3). We discuss our results in Section 7 and summarize our main findings in Section 8.

## 2 METHOD: PHYSICAL PROCESSES IN MULTIPLES AND IN TERTIARY-INDUCED MERGERS

We present our method using the evolutionary scenario depicted in Figure 4; this is appropriate for the production of GW190412-like events (see Section 3). However, with small adaption, this can be applied to GW190814 (see Section 4) and GW190521 (Section 5).

### 2.1 Supernova, Natal kick and Merger kick in Triple Systems

In our “primordial” scenario for the formation of merging BHBs (see leftmost pathway in Figures 1-3), the orbital parameters of the final BHB depend on the previous stellar/binary evolutionary history. Consider the inner triple system depicted in Figure 4. Since the orbital parameters may change due to SN explosion, we denote the pre-kick and post-kick orbital parameters using the superscripts “0” and “k”, respectively. The pre-SN relative velocity and separation distance of the inner binary and middle binary are denoted by  $\mathbf{v}_{\text{in}}^0$ ,  $\mathbf{r}_{\text{in}}^0$ ,  $\mathbf{v}_{\text{mid}}^0$ , and  $\mathbf{r}_{\text{mid}}^0$ , respectively. We have

$$|\mathbf{v}_{\text{in}}^0| = \sqrt{Gm_{12}^0 \left( \frac{2}{|\mathbf{r}_{\text{in}}^0|} - \frac{1}{a_{\text{in}}^0} \right)}, \quad (1)$$

$$|\mathbf{v}_{\text{mid}}^0| = \sqrt{Gm_{123}^0 \left( \frac{2}{|\mathbf{r}_{\text{mid}}^0|} - \frac{1}{a_{\text{mid}}^0} \right)}, \quad (2)$$

and the angular momenta of two orbits are given by

$$\mathbf{L}_{\text{in}}^0 \equiv \mu_{\text{in}}^0 \mathbf{h}_{\text{in}}^0 = \mu_{\text{in}}^0 (\mathbf{r}_{\text{in}}^0 \times \mathbf{v}_{\text{in}}^0), \quad (3)$$

$$\mathbf{L}_{\text{mid}}^0 \equiv \mu_{\text{mid}}^0 \mathbf{h}_{\text{mid}}^0 = \mu_{\text{mid}}^0 (\mathbf{r}_{\text{mid}}^0 \times \mathbf{v}_{\text{mid}}^0), \quad (4)$$

where  $\mu_{\text{in}}^0 \equiv m_1^0 m_2^0 / m_{12}^0$  (with  $m_{12}^0 = m_1^0 + m_2^0$ ),  $\mu_{\text{mid}}^0 \equiv m_{12}^0 m_3^0 / m_{123}^0$  (with  $m_{123}^0 = m_1^0 + m_2^0 + m_3^0$ ) are the reduced mass for the inner binary and middle binary, and  $\mathbf{h}_{\text{in}}^0$  and  $\mathbf{h}_{\text{mid}}^0$  are the specific angular momenta.

As a star explodes in a SN, it suffers a mass loss  $\Delta m$  and experiences a kick. We assume that the velocity of the natal kick ( $\mathbf{v}_k$ ) is drawn from a Maxwellian distribution

$$p(v_k) \propto v_k^2 e^{-v_k^2 / \sigma^2} \quad (5)$$

with a velocity dispersion  $\sigma$ . We also assume the kick direction is isotropically distributed. The natal kick on the first generation BH is highly uncertain, ranging from 0 km s<sup>-1</sup> to  $\sim 100$  km s<sup>-1</sup> (e.g., Repetto & Nelemans 2015; Mandel 2016). We will consider both extreme values (0 and 100 km s<sup>-1</sup> in our study. On the other hand, the kick velocity on a newly formed NS (relevant to GW190814) is well constrained and we adopt  $\sigma = 260$  km s<sup>-1</sup> (e.g., Hobbs et al. 2005).

We assume the first SN explosion takes place on the primary star in the inner binary, and the newly born BH loses 10% of the mass due to neutrino emission. The mass of the remnant becomes  $m_1^k = m_1^0 - \Delta m$ . The natal kick takes place instantaneously compared to the orbital period. Thus, the relative velocity of the inner binary is  $\mathbf{v}_{\text{in}}^k = \mathbf{v}_{\text{in}}^0 + \mathbf{v}_{k1}$

(where  $|\mathbf{v}_{k1}| = v_{k1}$ ; see Equation 5). Since  $\mathbf{r}_{\text{in}}^k = \mathbf{r}_{\text{in}}^0$ , the post-SN semimajor axis is given by

$$a_{\text{in}}^k = \left( \frac{2}{|\mathbf{r}_{\text{in}}^k|} - \frac{|\mathbf{v}_{\text{in}}^k|^2}{G(m_1^k + m_2^0)} \right)^{-1}, \quad (6)$$

and the post-SN eccentricity can be obtained from the Laplace-Runge-Lenz vector

$$\mathbf{e}_{\text{in}}^k = \frac{1}{G(m_1^k + m_2^0)} (\mathbf{v}_{\text{in}}^k \times \mathbf{h}_{\text{in}}^k) - \frac{\mathbf{r}_{\text{in}}^k}{|\mathbf{r}_{\text{in}}^k|}, \quad (7)$$

where  $\mathbf{h}_{\text{in}}^k = \mathbf{r}_{\text{in}}^k \times \mathbf{v}_{\text{in}}^k$ .

Note that the SN on  $m_1^0$  also imparts a kick on the center of mass (CM) of the inner binary, which can change the orbital parameters of the middle and outer orbits. If we define the velocity vector of individual body as  $\mathbf{v}_{1,2,3}^0$ , respectively, we have  $\mathbf{v}_{\text{mid}}^0 = \mathbf{v}_3^0 - \mathbf{v}_{12\text{cm}}^0$ , where  $\mathbf{v}_{12\text{cm}}^0 \equiv (m_1^0 \mathbf{v}_1^0 + m_2^0 \mathbf{v}_2^0)/m_{12}^0$  is the velocity of the CM of the inner binary. As  $m_1^0$  experiences SN,  $\mathbf{v}_1^k = \mathbf{v}_1^0 + \mathbf{v}_{k1}$ , the post-SN relative velocity of the middle binary becomes (e.g., [Pijloo et al. 2012](#))

$$\begin{aligned} \mathbf{v}_{\text{mid}}^k &= \mathbf{v}_3^0 - \mathbf{v}_{12\text{cm}}^k \\ &= \mathbf{v}_{\text{mid}}^0 - \frac{m_2^0(m_1^k - m_1^0)}{m_{12}^0(m_1^k + m_2^0)} \mathbf{v}_{\text{in}}^0 - \frac{m_1^k}{m_1^k + m_2^0} \mathbf{v}_{k1}, \end{aligned} \quad (8)$$

and the specific angular momentum of the middle binary is given by  $\mathbf{h}_{\text{mid}}^k = \mathbf{r}_{\text{mid}}^k \times \mathbf{v}_{\text{mid}}^k$ . The post-SN  $a_{\text{mid}}^k$  and  $\mathbf{e}_{\text{mid}}^k$  can be evaluated by replacing  $\mathbf{r}_{\text{in}}^k \rightarrow \mathbf{r}_{\text{mid}}^k$ ,  $\mathbf{v}_{\text{in}}^k \rightarrow \mathbf{v}_{\text{mid}}^k$ ,  $\mathbf{h}_{\text{in}}^k \rightarrow \mathbf{h}_{\text{mid}}^k$  and  $(m_1^k + m_2^0) \rightarrow (m_1^k + m_2^0 + m_3^0)$  in Equations (6)-(7).

The orientations of the angular momenta of two (inner and middle) orbits can change as a consequence of the natal kick. Taking the middle binary as an example, the angle between the pre-kick and post-kick angular momentum can be computed by

$$\Delta I_{\text{mid}} = \arccos(\hat{\mathbf{h}}_{\text{mid}}^0 \cdot \hat{\mathbf{h}}_{\text{mid}}^k), \quad (9)$$

where  $\hat{\mathbf{h}}$  is the unit vector. Note that if the system goes through multiple kicks, the final angular momentum orientation may change a lot with respect to the original one.

Similar prescriptions can be applied to the cases where the SN explosion takes place on  $m_2$  and  $m_3$ .

Once the inner BH binary merges, the remnant ( $m_{12}$ ) will receive a merger kick. Assuming the two BHs ( $m_1$  and  $m_2$ ) have negligible spins ( $\chi_1 = \chi_2 \ll 1$ ), the kick velocity on  $m_{12}$  is given by the fitting formula (e.g., [Lousto et al. 2010](#))

$$V_{\text{mk}} = 1.2 \times 10^4 \text{ km s}^{-1} \left[ \frac{\eta^2(1 - m_2/m_1)}{1 + m_2/m_1} (1 - 0.93\eta) \right], \quad (10)$$

where  $\eta \equiv (m_2/m_1)/(1 + m_2/m_1)^2$ . This merger kick is along the random direction in the inner orbital plane. The response of the middle binary due to this kick is analogous to the change in the inner binary that has experienced a natal kick on one component. The GW emission in the BHB merger is accompanied by energy (“mass”) loss, given by

$$\frac{\delta m}{m_1 + m_2} = 0.057\eta + 0.445\eta^2 + 0.522\eta^3. \quad (11)$$

The final remnant spin is given by

$$\chi_{12} = \frac{3.46\eta - 4.34\eta^2 + 1.69\eta^3}{(1 - 0.06\eta - 0.44\eta^2 - 0.52\eta^3)^2}. \quad (12)$$

## 2.2 Tertiary-Induced Mergers: Analytical Results

Regardless how the “final” BHB (the middle binary in Figure 4) is produced (either in the “primordial” pathway or in one of the “interaction” pathways, see Figures 1-3), it would have too large an orbital separation to merge by itself in most situations. Instead, the middle binary (with mass  $m_{12}$  and  $m_3$ ) can be driven to merge due to the gravitational perturbation from the external body ( $m_4$ , MBH) that moves on an inclined outer orbit relative to the orbit of the middle binary. The LK mechanism induces oscillations in the eccentricity and inclination of the middle binary on the timescale

$$T_{\text{LK}} = \frac{1}{n_{\text{mid}}} \frac{m_{12} + m_3}{m_4} \left( \frac{a_{\text{out,eff}}}{a_{\text{mid}}} \right)^3, \quad (13)$$

where  $n_{\text{mid}} = [G(m_{12} + m_3)/a_{\text{mid}}^3]^{1/2}$  is the mean motion of the middle binary, and

$$a_{\text{out,eff}} \equiv a_{\text{out}} \sqrt{1 - e_{\text{out}}^2} \quad (14)$$

is the effective outer binary semi-major axis.

During LK oscillations, the short-range force effects (such as GR-induced apsidal precession) play a crucial role in limiting the maximum eccentricity  $e_{\text{max}}$  of the middle binary (e.g., [Fabrycky & Tremaine 2007](#)). In the absence of energy dissipation, the evolution of the triple is governed by two conservation laws: the total orbital angular momentum and the total energy of the system. An analytical expression for  $e_{\text{max}}$  for general hierarchical triples (arbitrary masses and eccentricities) can be obtained in the double-averaged secular approximation if the disturbing potential is truncated to the quadrupole order (i.e., when the octupole-order perturbation is negligible; see below). Using the method of [Liu et al. \(2015\)](#) (see also [Anderson et al. 2016, 2017](#)), we find

$$\begin{aligned} &\frac{3}{8} \left\{ j_{\text{min}}^2 - j_0^2 + (5 - 4j_{\text{min}}^2) \right. \\ &\left[ 1 - \frac{((j_{\text{min}}^2 - j_0^2)\eta - 2j_0 \cos I_0)^2}{4j_{\text{min}}^2} \right] \\ &\left. - (1 + 4e_0^2 - 5e_0^2 \cos^2 \omega_0) \sin^2 I_0 \right\} + \varepsilon_{\text{GR}} (j_0^{-1} - j_{\text{min}}^{-1}) = 0, \end{aligned} \quad (15)$$

where  $e_0$ ,  $I_0$  and  $\omega_0$  are the initial eccentricity<sup>1</sup>, inclination and longitude of the periape of the middle binary, respectively, and we have defined  $j_{\text{min}} \equiv \sqrt{1 - e_{\text{max}}^2}$ ,  $j_0 \equiv \sqrt{1 - e_0^2}$ ,  $\eta \equiv |\mathbf{L}_{\text{mid}}|/|\mathbf{L}_{\text{out}}|$  (at  $e_0 = 0$ ), and

$$\varepsilon_{\text{GR}} = \frac{3G(m_{12} + m_3)^2 a_{\text{out,eff}}^3}{c^2 a_{\text{mid}}^4 m_4}. \quad (16)$$

<sup>1</sup> We denote the initial values of parameters for LK oscillations using the subscript “0”. Note that the superscript “0” refers to the pre-SN parameters (see Section 2.2).



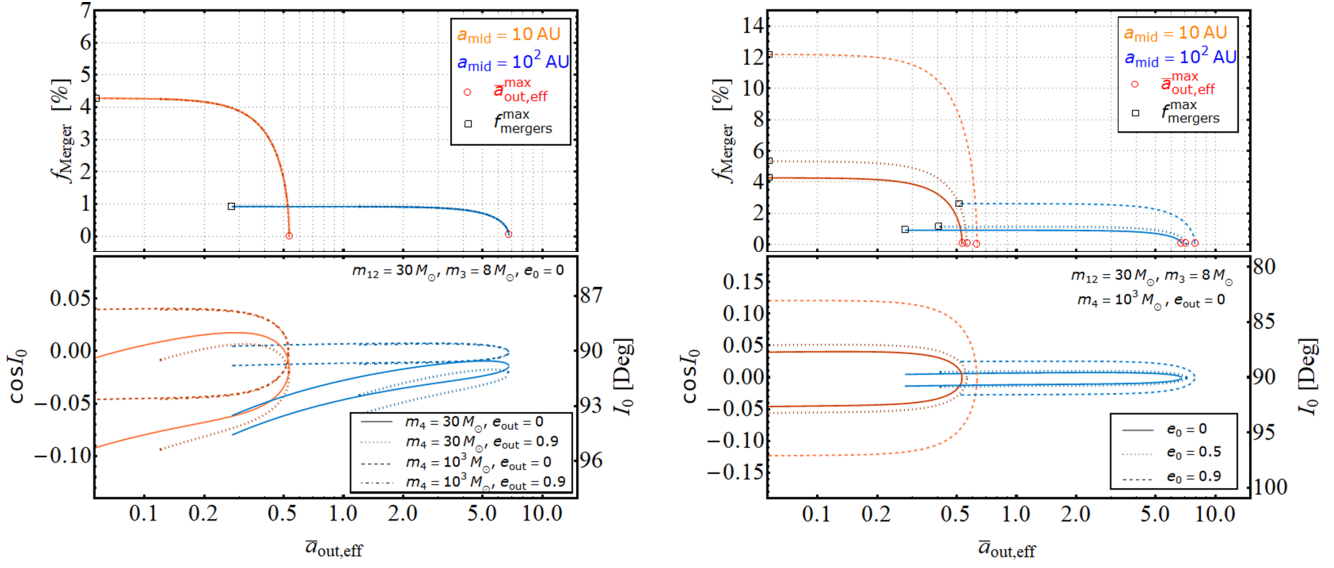


**Figure 5.** Merger fractions and merger windows (see Equation 24) as a function of  $\bar{a}_{\text{out,eff}}$  (see Equation 25) for LK-induced mergers. In this sample plot, we consider the induced merger of the middle binary (with component masses  $m_{12} = 30M_{\odot}$  and  $m_3 = 8M_{\odot}$ ) by a tertiary  $m_4$ . In the left panels, the middle binary has an initially circular orbit (i.e., initial  $e_{\text{mid}} = e_0 = 0$ , and two different initial  $a_{\text{mid}}$ 's) and we choose different tertiary companions as labeled. In the right panels, we fix the tertiary companion mass and eccentricity ( $m_4 = 10^3 M_{\odot}$ ,  $e_{\text{out}} = 0$ ) but vary the initial eccentricity  $e_0$  of the middle binary (as labeled). These results are obtained analytically using Equations (15), (23) and (24). Each curve terminates on the left at the instability limit. The maximum value of  $\bar{a}_{\text{out,eff}}$  to have a merger is denoted by  $\bar{a}_{\text{out,eff}}^{\text{max}}$  (Equation 27), and the maximum value of  $f_{\text{merger}}$  (which occurs at small  $\bar{a}_{\text{out,eff}}$ ) is denoted by  $f_{\text{merger}}^{\text{max}}$  (Equation 26).

Note that for  $e_0 = 0$ , Equation (15) reduces to Equation (24) of Anderson et al. (2017). For the general  $\eta$ , the maximum possible  $e_{\text{max}}$  for all values of  $I_0$ , called  $e_{\text{lim}}$ , is given by (assuming  $\omega_0 = 0$ )

$$\frac{3}{8} \left[ 5 - 2j_0^2 - 3j_{\text{lim}}^2 + \frac{\eta^2}{4} \left( \frac{4}{5} j_{\text{lim}}^2 - 1 \right) \frac{(j_{\text{lim}}^2 - j_0^2)^2}{j_{\text{lim}}^2 - 1} \right] + \varepsilon_{\text{GR}} (j_0^{-1} - j_{\text{lim}}^{-1}) = 0, \quad (17)$$

where  $j_{\text{lim}} \equiv \sqrt{1 - e_{\text{lim}}^2}$ .

For systems with  $m_{12} \neq m_3$  and  $e_{\text{out}} \neq 0$ , so that

$$\varepsilon_{\text{oct}} \equiv \frac{m_{12} - m_3}{m_{12} + m_3} \left( \frac{a_{\text{mid}}}{a_{\text{out}}} \right) \frac{e_{\text{out}}}{1 - e_{\text{out}}^2} \quad (18)$$

is non-negligible, the octupole effect may become important (e.g., Ford et al. 2000; Naoz 2016). This tends to widen the inclination window for large eccentricity excitation. However, the analytic expression for  $e_{\text{lim}}$  given by Equation (17) remains valid even for  $\varepsilon_{\text{oct}} \neq 0$  (e.g., Liu et al. 2015; Anderson et al. 2017). In other words, because of the effect of short-range forces due to GR, the maximum eccentricity cannot exceed  $e_{\text{lim}}$  even when the octupole potential is significant. Note that the stability of triple systems requires (e.g., Kiseleva et al. 1996)

$$\frac{a_{\text{out}}(1 - e_{\text{out}})}{a_{\text{mid}}(1 + e_{\text{mid}})} > \frac{3.7}{Q_{\text{out}}} - \frac{2.2}{1 + Q_{\text{out}}} + \frac{1.4}{Q_{\text{in}}} \frac{Q_{\text{out}} - 1}{Q_{\text{out}} + 1}, \quad (19)$$

where  $Q_{\text{in}} = [\max(m_{12}, m_3)/\min(m_{12}, m_3)]^{1/3}$  and  $Q_{\text{out}} = (m_{123}/m_4)^{1/3}$ . In the limit of  $m_4 \gg m_{123}$ , Equation (19) reduces to  $[a_{\text{out}}(1 - e_{\text{out}})/a_{\text{mid}}(1 + e_{\text{mid}})] \gtrsim [3.7(m_4/m_{123})^{1/3}]$ .

This implies

$$\begin{aligned} \varepsilon_{\text{oct}} &\lesssim \left( \frac{m_{12} - m_3}{m_{123}} \right) \frac{1}{3.7} \left( \frac{m_{123}}{m_4} \right)^{1/3} \frac{e_{\text{out}}}{(1 + e_{\text{out}})(1 + e_{\text{mid}})} \\ &\lesssim 1.5 \times 10^{-3} \left( \frac{m_{12} - m_3}{m_{123}} \right) \left( \frac{10^5 m_{123}}{m_4} \right)^{1/3}, \end{aligned} \quad (20)$$

where in the second line we have used  $e_{\text{out}}/(1 + e_{\text{out}}) \leq 1/2$  and set  $e_{\text{mid}} \simeq 1$  (since merger requires high eccentricity). Therefore,  $\varepsilon_{\text{oct}} \lesssim 0.001$  when  $m_4/m_{123} \gtrsim 10^5$ . For such systems, the  $e$ -excitation window is very similar to the quadrupole result (e.g., Liu et al. 2015; Muñoz et al. 2016; Liu et al. 2019b). Only a small fraction of mergers are influenced by the octupole effect.

In tertiary-induced mergers, when the octupole effect is negligible, the merger time can be well approximated by (e.g., Wen 2003; Thompson 2011; Liu & Lai 2018)

$$T_{\text{m}} \simeq T_{\text{m},0} (1 - e_{\text{max}}^2)^3, \quad (21)$$

where

$$T_{\text{m},0} \equiv \frac{5c^5 a_{\text{mid},0}^4}{256G^3 (m_{12} + m_3)^2 \mu_{\text{mid}}} \quad (22)$$

is the merger time due to GW emission for an isolated circular BHB, and  $e_{\text{max}}$  is from Equation (15)<sup>2</sup>. Using Equation

<sup>2</sup> Note that Equation (21) only applies in the quadrupole approximation, which is valid for  $m_4 \gg m_{123}$ . Hoang et al. (2018) considered BHBs around a SMBH, and found numerical examples where a fraction of BHBs has the merger time shorter than pre-

(21), we can define the “merger eccentricity”  $e_m$  via

$$T_{m,0}(1 - e_m^2)^3 = T_{\text{crit}}. \quad (22)$$

Thus, only systems with  $e_{\text{max}} \gtrsim e_m$  can have the merger time  $T_m$  less than  $T_{\text{crit}}$ . We typically set  $T_{\text{crit}} = 1.4 \times 10^{10}$  yrs in this paper. However, for triple systems located in dense star clusters, such timescale decreases due to the effects from the surrounding stars (see Section 7.2). Note that our numerical calculations show that Equation (23) is approximately valid as long as  $e_0 \lesssim 0.9$ . Combining Equations (15) and (23), the merger window (bounded by the critical inclination angles  $I_{0,\text{merger}}^\pm$ ) can be obtained that allows the middle binary to attain  $e_m$  and merge within  $T_{\text{crit}}$ . If we assume the orbital orientation of tertiary companion is distributed isotropically, the merger fraction of the BHB is given by (see Section 3 in Liu & Lai 2018)

$$f_{\text{merger}} = \frac{1}{2} \left| \cos I_{0,\text{merger}}^+ - \cos I_{0,\text{merger}}^- \right|. \quad (24)$$

Since the eccentricity excitation depends on  $m_4$  (the MBH),  $a_{\text{out}}$ ,  $e_{\text{out}}$  through the ratio  $m_4/(a_{\text{out}}\sqrt{1 - e_{\text{out}}})^3$  in the quadrupole approximation, we introduce the dimensionless scaled semi-major axis

$$\bar{a}_{\text{out,eff}} = \left( \frac{a_{\text{out}}\sqrt{1 - e_{\text{out}}}}{1000\text{AU}} \right) \left( \frac{m_4}{10M_\odot} \right)^{-1/3} \quad (25)$$

to characterize the “strength” of the external perturber.

Figure 5 presents the results of the merger fraction and merger window for BHB ( $m_{12} = 30M_\odot$  and  $m_3 = 8M_\odot$ ) as a function of  $\bar{a}_{\text{out,eff}}$ , obtained using Equations (15), (23)-(25) and  $T_{\text{crit}} = 1.4 \times 10^{10}$  yrs. All the systems shown here satisfy the stability criterion for the triples (e.g., Kiseleva et al. 1996). We choose two different initial semi-major axes ( $a_{\text{mid}} = 10\text{AU}$  and  $100\text{AU}$ ). In the left panels, for each BHB, we fix the initial eccentricity of the middle BHB to zero and consider a variety of outer binaries (different  $m_4$  and  $e_{\text{out}}$ , as labeled). We find that, for a given  $a_{\text{mid}}$ , different  $m_4$  and  $e_{\text{out}}$  (with the same  $\bar{a}_{\text{out,eff}}$ ) affect the position of merger window (i.e. the range of  $\cos I_0$ ) but not the value of  $f_{\text{merger}}$ . We see that  $f_{\text{merger}}$  is approximately constant until  $\bar{a}_{\text{out,eff}}$  is close to a maximum value ( $\bar{a}_{\text{out,eff}}^{\text{max}}$ ), beyond which  $f_{\text{merger}}$  quickly drops to zero. Also, the merger window and fraction have strong dependence on the initial semi-major axis ( $a_{\text{mid}}$ ). This is because for small  $a_{\text{mid}}$ , the induced eccentricity in the LK oscillations does not have to be too large to produce mergers within  $T_{\text{crit}}$ . In the right panels, we fix the outer binary and consider the effect of different  $e_0$  (the initial value of  $e_{\text{mid}}$ ). We find that the merger window and fraction can be increased by a factor of a few if the BHB is initialized as an eccentric orbit. In addition, we see that the range of  $\bar{a}_{\text{out,eff}}$  producing merger is different for different separation of BHBs.

dicted by Equation (21). This is because their examples refer to BHBs very close to the SMBH, and the systems are near the instability limit. In any case, only a small fraction of mergers are influenced by the octuple effect.

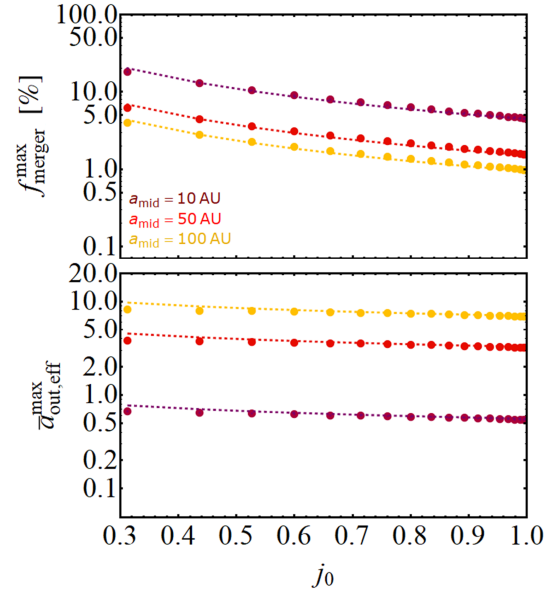


**Figure 6.** The maximum values of  $f_{\text{merger}}$  and  $\bar{a}_{\text{out,eff}}$  (see Figure 5) as a function of  $j_0 = \sqrt{1 - e_0^2}$  of the BHB (the middle binary). The points are obtained analytically using Equations (15), (23) and (24). The dashed lines are given by the fitting formulae (26) and (27).

In Liu & Lai (2018) (see their Equations 53-54), we showed that the maximum merger fraction  $f_{\text{merger}}^{\text{max}}$  (i.e., the maximum value of  $f_{\text{merger}}$  for a given initial  $a_{\text{mid}}$ ) and  $\bar{a}_{\text{out,eff}}^{\text{max}}$  (the maximum value of  $\bar{a}_{\text{out,eff}}$  beyond which  $f_{\text{merger}}$  drops to zero) can be characterized by two simple fitting formulas when the BHB is initialized in a circular orbit (initial  $e_{\text{mid}} = 0$ ). Here, we extend the fittings to cover BHBs with different initial eccentricities. From Equation (23), we see that the critical eccentricity  $e_m$  required for merger within time  $T_{\text{crit}}$  depends on  $(\mu_{\text{mid}}T_{\text{crit}})(m_{123}/a_{\text{mid}}^2)^2$  for initial  $e_{\text{mid}} = 0$ , where  $m_{123} = m_{12} + m_3$  and  $\mu_{\text{mid}} = m_{12}m_3/m_{123}$ . From Equation (15) we see that the critical inclinations for a given  $e_{\text{max}} = e_m$  depend on  $\varepsilon_{\text{GR}}$ , or the combination  $(m_{123}/a_{\text{mid}}^2)^2(a_{\text{out,eff}}^3/m_4)$ , and  $j_0 = \sqrt{1 - e_0^2}$ . Thus the merger fraction  $f_{\text{merger}}$  depends on  $m_{12}$ ,  $m_3$ ,  $a_{\text{mid}}$ ,  $e_0$  and  $T_{\text{crit}}$  only through  $j_0$ ,  $m_{123}/a_{\text{mid}}^2$  and  $\mu_{\text{mid}}T_{\text{crit}}$ . Based on these, we expect that  $f_{\text{merger}}^{\text{max}} \propto j_0^\alpha (a_{\text{mid}}/m_{123}^{0.5})^{-0.67} (\mu_{\text{mid}}T_{\text{crit}})^{0.16}$  and  $\bar{a}_{\text{out,eff}}^{\text{max}} \propto j_0^\beta (a_{\text{mid}}/m_{123}^{0.5})^{1.1} (\mu_{\text{mid}}T_{\text{crit}})^{0.06}$ , where  $\alpha$ ,  $\beta$  are fitting parameters. Figure 6 shows that  $\alpha = -1.3$  and  $\beta = -0.28$  provide good fit. Thus we have

$$f_{\text{merger}}^{\text{max}} \simeq 4.35\% (1 - e_0^2)^{-0.65} \left( \frac{\mu_{\text{mid}}}{M_\odot} \frac{T_{\text{crit}}}{10^{10}\text{yrs}} \right)^{0.16} \times \left[ \left( \frac{a_{\text{mid}}}{\text{AU}} \right) \left( \frac{m_{12} + m_3}{M_\odot} \right)^{-0.5} \right]^{-0.67}, \quad (26)$$

and

$$\bar{a}_{\text{out,eff}}^{\text{max}} \simeq 0.29 (1 - e_0^2)^{-0.14} \left( \frac{\mu_{\text{mid}}}{M_\odot} \frac{T_{\text{crit}}}{10^{10} \text{yrs}} \right)^{0.06} \times \left[ \left( \frac{a_{\text{mid}}}{\text{AU}} \right) \left( \frac{m_{12} + m_3}{M_\odot} \right)^{-0.5} \right]^{1.1} \quad (27)$$

These fitting formulae are valid for any type of LK-induced BH mergers in the quadrupole order (which is valid when the tertiary is a MBH; see [Liu & Lai \(2018\)](#) for how octupole effects can increase the merger fraction).

### 3 FORMATION OF GW190412

In this section, we examine the formation of GW190412 in the “primordial multiple” scenario (see Figure 4 and the leftmost pathway of Figure 1). The formation of the “final” binary due to dynamical interactions is discussed in Section 6.

#### 3.1 Properties of the Inner Binary

In our scenario (Figures 1 and 4), GW190412 is a tertiary-induced merger, where the primary component ( $m_{12}$ ) in the middle binary is itself the merger product of an inner binary ( $m_1$  and  $m_2$ ). Since the spin magnitude of the “second generation (2G) BH” ( $\chi_{12}$ ) in this source has already been determined ( $\chi_{12} = 0.43^{+0.16}_{-0.26}$ ; [Abbott et al. 2020a](#)), the mass ratio of two progenitors can be constrained if the 1G BHs have negligible spins — this is reasonable if  $m_1$  and  $m_2$  are a natural product of stellar/binary evolution (e.g., [Fuller et al. 2019](#); [Fuller & Ma 2019](#)).

In Figure 7, we use Equations (10), (12) and plot the merger kick ( $V_{\text{mk}}$ ) and spin ( $\chi_{12}$ ) as a function of  $m_2/m_1$ , assuming no natal spin for the two 1G BHs (see black curves). For reference, if each 1G BH has a small but finite spin ( $\chi_1, \chi_2 \lesssim 0.1$ ) and the associated spin orientation is aligned with the orbital angular momentum, the values of  $V_{\text{mk}}$  and  $\chi_{12}$  (obtained by the analytic fits in [Lousto et al. \(2010\)](#)) would exhibit only small spread (see the red band in Figure 7). Using the observed value of  $\chi_{12} = 0.43^{+0.16}_{-0.26}$ , the mass ratio is constrained to be  $m_2/m_1 = 0.211^{+0.208}_{-0.153}$ . For concreteness, we adopt  $m_{12} = 30M_\odot$ , and introduce three cases to cover the possible range for the parameters of the progenitors of  $m_{12}$  (see Table 1). Note that we have included the radiated energy from GW on the component masses (see Equation 11); thus  $m_{12} = m_1 + m_2 - \delta m$ .

#### 3.2 Constrain the post-kick orbit of BHB (the middle binary)

Having obtained the possible masses ( $m_1, m_2$ ) of the inner binary from the GW data on GW190412, (Section 3.1), we now constrain what kind of middle binary ( $m_{12} = 30M_\odot$  around  $m_3 = 8M_\odot$ ) can survive the three SNs and the merger kick without becoming unbound. In our fiducial example, we adopt the parameters in Case I (see Table 1),

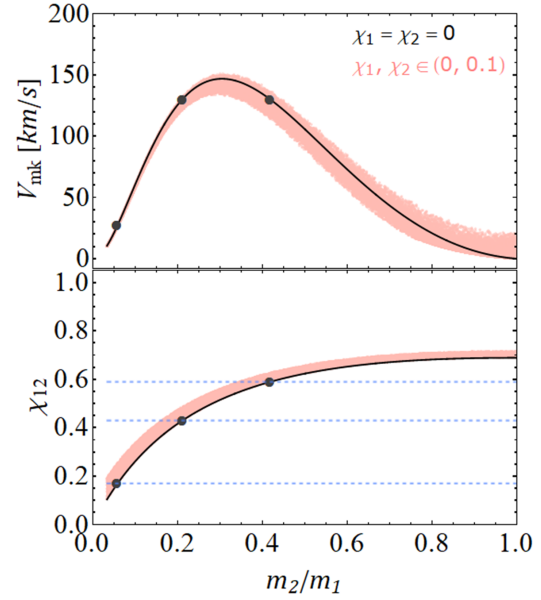


**Figure 7.** The merger kick (upper panel) and remnant spin (lower panel) as a function of binary mass ratio. The solid lines are from Equations (10) and (12) for  $\chi_1 = \chi_2 = 0$ , and the red bands are obtained assuming progenitors are slowly rotating with  $\chi_1, \chi_2 \lesssim 0.1$  (see the analytic fits in [Lousto et al. \(2010\)](#)). The dashed-blue lines in the lower panel indicate the range of the observed spin magnitude of the primary component of GW190412, i.e.,  $\chi_{12} = 0.43^{+0.16}_{-0.26}$ . From this, the mass ratio of the progenitors and the kick velocity can be constrained. The black dots indicate the three cases shown in Table 1.

**Table 1.** Possible parameters of the progenitors of the  $30M_\odot$  primary in GW190412, following the constraints from Figure 7.

	Case I	Case II	Case III
$\chi_{12}$	0.43	0.17	0.59
$m_2/m_1$	0.211	0.058	0.419
$m_1, m_2 [M_\odot]$	25.2, 5.3	28.5, 1.6	21.9, 9.2
$V_{\text{mk}} [\text{km/s}]$	130	27.1	129.8

and assume the natal kick is negligible ( $\sigma_{\text{BH}} = 0 \text{ km s}^{-1}$  in Equation 5). In our scenario,  $m_1$  and  $m_2$  merge through the standard binary evolution channel<sup>3</sup>. So we choose  $a_{\text{in}}^0 = 0.1 \text{ AU}$  and  $e_{\text{in}}^0 = 0$  at the initial time (right before the SN explosion). These are reasonable in the standard binary evolution model (e.g., [Belczynski et al. 2016](#)), although a range of the initial values of  $a_{\text{in}}^0$  are possible. Our choice of  $a_{\text{in}}^0$  only affects  $a_{\text{mid}}$ ,  $e_{\text{mid}}$  through the stability requirement for the inner triple (see below). Our strategy for constraining the middle binary is as follows:

<sup>3</sup> The innermost binary may also merge due to the perturbation from  $m_3$  through LK oscillations. But this process depends on the mutual inclination angle as well as several additional effects on  $m_1$  and  $m_2$  during the stellar evolution, i.e., tidal effect and mass transfer, which can suppress the eccentricity excitation.



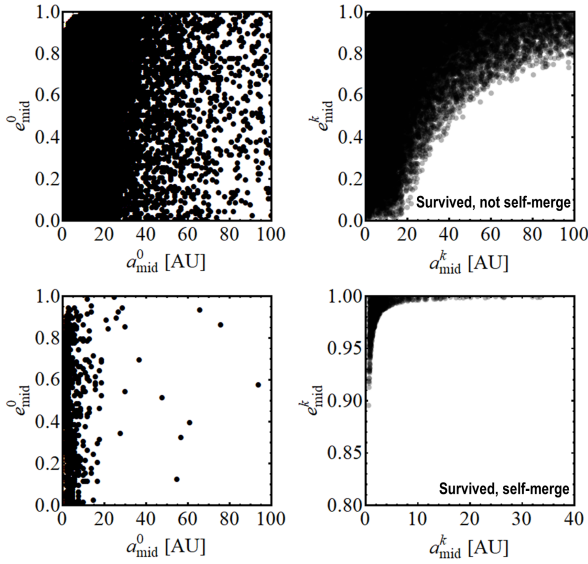


**Figure 8.** The distributions of  $a_{\text{mid}}$  and  $e_{\text{mid}}$  for the survived middle binaries that have undergone four kicks (three natal kicks and one merger kick), where the right panels show the post-kick systems while the left panels show their pre-kick precursors. The post-kick middle binaries in the upper right panel cannot merge within the Hubble time by themselves, while the survived binaries in the lower right panel can. In our calculation, the pre-kick component masses are chosen to be  $m_1^0 = 28M_\odot$ ,  $m_2^0 = 5.9M_\odot$  and  $m_3^0 = 8.9M_\odot$  and post-kick masses are  $m_1^k = 25.2M_\odot$ ,  $m_2^k = 5.3M_\odot$  (Case I in Table 1) and  $m_3^k = 8M_\odot$ . Note that the pre-SN mass is larger than the post-SN mass by about 10%. The natal kicks for each newly born BH is assumed to be negligible ( $\sigma_{\text{BH}} = 0 \text{ km s}^{-1}$ ) but the merger kick is set to be  $V_{\text{mk}} = 130 \text{ km s}^{-1}$  (see Table 1).

- We sample a  $100 \times 100$  uniform grid in the plane of  $a_{\text{mid}}^0 - e_{\text{mid}}^0$ , with the pre-SN semi-major axis  $a_{\text{mid}}^0$  ranging from 0 to 100 AU, and eccentricity  $e_{\text{mid}}^0$  ranging from 0 to 1. This parameter space is further constrained by the stability criterion (e.g., Kiseleva et al. 1996) for the inner triple system ( $m_1, m_2, m_3$ ). Note that in principle, the initial middle binaries may have a wider range of  $a_{\text{mid}}^0$  (e.g., to  $10^4$  AU or larger in the galactic field). Such wide binaries ( $a_{\text{mid}}^0 \gtrsim 100$  AU) are much less common: e.g., in the galactic field, the typical semi-major axis distribution is roughly  $\propto (a_{\text{mid}}^0)^{-1.5}$  or steeper (see Moe & Di Stefano 2017; El-Badry & Rix 2018; Tian et al. 2020); the distribution in dense star cluster is unknown. Moreover, such wide binaries can be easily destroyed by various kicks (see below). Since our main goal is to determine the range of  $a_{\text{mid}}$ ,  $e_{\text{mid}}$  for the survived middle binaries, it is not important to sample larger values of  $a_{\text{mid}}^0$ .

- For each allowed (i.e. stable) triple system (specified by the values of  $a_{\text{mid}}^0$  and  $e_{\text{mid}}^0$ ), we let SN occur on each mass component and the merger kick on  $m_{12}$ , following the sequence shown in Figure 4. Every time a kick happens, we draw a random orbital phase (uniform distribution of the orbital mean anomaly), and only keep the stable post-kick systems. In order for  $m_1$  and  $m_2$  to merge within the

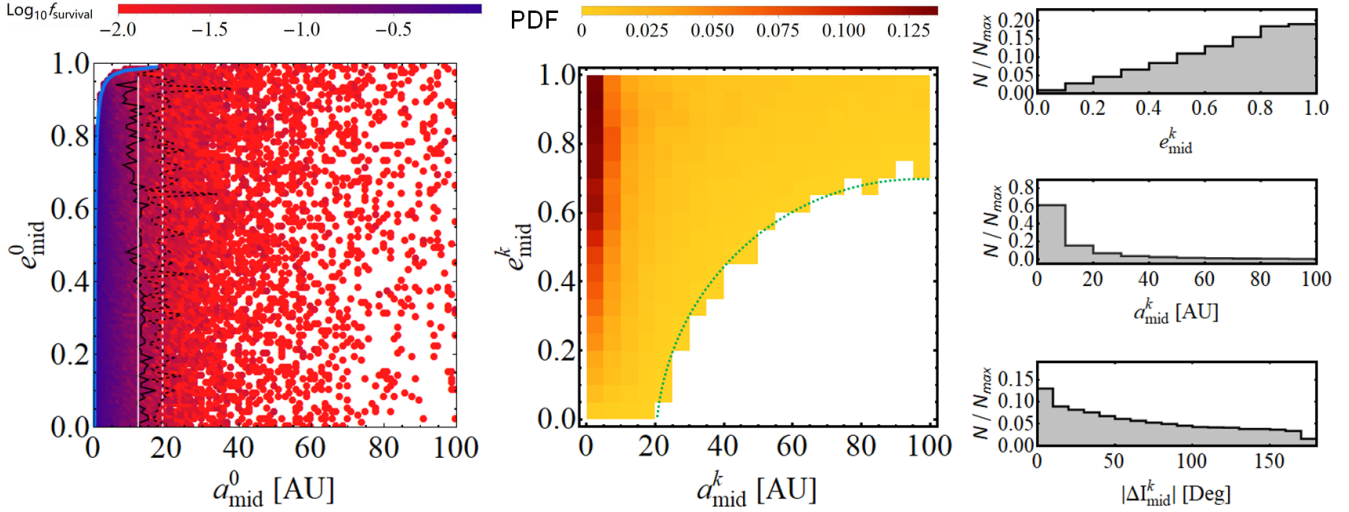
Hubble time by themselves, we also remove systems that have a longer merger time ( $\gtrsim 1.4 \times 10^{10}$  yrs) when both  $m_1$  and  $m_2$  become BHs.

- Since the changes of the orbital parameters depend on the orientations of the kick velocities (i.e., natal kick has a random orientation, and merger kick is in the orbital plane), to cover all possibilities, we repeat the previous step for 100 times for each  $(a_{\text{mid}}, e_{\text{mid}})$ . Thus, the statistical features of the survivals can be characterized by the accumulated data.

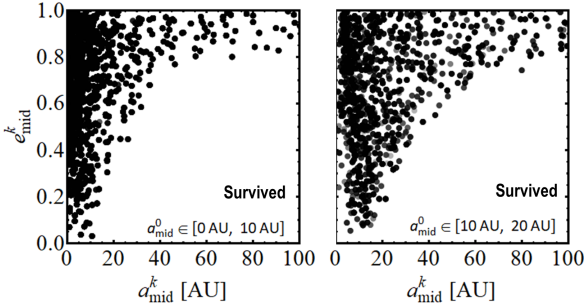
Figure 8 shows the distributions of the survived binaries (right panels) and their progenitors (left panels) that have undergone 3 natal kicks and one merger kick. We separate the post-kick systems into two categories: the survived middle binaries that cannot merge over the cosmic time by themselves (upper panels) and those that can (lower panels). In the upper left panel, we exhibit the pre-kick distributions of  $a_{\text{mid}}^0$  and  $e_{\text{mid}}^0$  for the survived binaries. We see that only the binaries with sufficiently small  $a_{\text{mid}}^0$  ( $\lesssim 40$  AU) can survive the SNs and kicks — binaries with larger  $a_{\text{mid}}^0$  are easily destroyed. In the upper right panel, we show the post-kick orbital parameters of survived middle binaries in the  $a_{\text{mid}}^k - e_{\text{mid}}^k$  plane. We see that these systems tend to have small  $a_{\text{mid}}^k$  and larger  $e_{\text{mid}}^k$ . Note that the kicks can either harden or soften the binary. In the bottom right panel, we find that some of the post-kick binaries in our simulations can merge within the Hubble time in isolation; these all have small separations and extreme large orbital eccentricities. Since the fraction of such systems is quite small ( $\sim 2\%$ ), we suggest that an external companion ( $m_4$ , MBH) is required to induce the merger of post-kick survived binaries.

Figure 9 shows the similar results as Figure 8, but includes all survived binaries. In the left panel, the blue line denotes the stability limit of the inner triples. Each dot implies that there is at least one successful survived binary, and the color represents the surviving possibility (as labeled). The systems with high survival fraction, where  $f_{\text{survival}} > 10\%$  (5%), are enclosed by solid-black (dashed-black) line. We also average the values of  $a_{\text{mid}}^0$  on these black (solid and dashed) lines and highlight them as the solid-white (dashed-white) lines to show the approximate boundaries. In the middle panel, we show the PDF of all post-kicks survived middle binaries. We find that the majority of survived systems cluster around the region with  $a_{\text{mid}}^k < 10$  AU and  $e_{\text{mid}}^k > 0.6$  (see the middle panel). We also present the distributions of the post-kick orbital parameters in the right panels. In the bottom rightmost panel, we show the change in the orientation of  $\mathbf{L}_{\text{mid}}$  after experiencing 4 kicks (from the initial  $\mathbf{L}_{\text{mid}}^0$ ). We see that  $|\Delta I_{\text{mid}}^k|$  has a broad range, indicating the orientation of  $\mathbf{L}_{\text{mid}}$  can change significantly.

To examine the dependence of the survived middle binaries on the initial semimajor axis, we show in Figure 10 the systems from two ranges of  $a_{\text{mid}}^0$ . We see that the final distributions of  $a_{\text{mid}}^k$  and  $e_{\text{mid}}^k$  have a weak dependence on the initial middle binary parameters. In another word, the



**Figure 9.** Same as Figure 8, but combining all survived middle binaries. The left panel shows the pre-kick systems that have been constrained by the stability criterion of the inner triple (assuming the pre-kick inner binary has  $a_{\text{in}}^0 = 0.1\text{AU}$ ) (solid-blue line), and the survival fractions are color-coded. The systems with  $f_{\text{survival}} > 10\%$  (5%) are enclosed by the black-solid (dashed) line, and the white (solid and dashed) lines represent the averages. The middle panel shows the post-kick systems that have survived; the PDF (color coded) denotes the distributions of  $a_{\text{mid}}^k$  and  $e_{\text{mid}}^k$ ; we see that most of the survived systems cluster around the parameter region with relative small  $a_{\text{mid}}^k$  and large  $e_{\text{mid}}^k$ . The green-dotted line represents an approximate boundary below which no system is produced. The three rightmost panels show the probability distribution of  $e_{\text{mid}}^k$ ,  $a_{\text{mid}}^k$  and  $|\Delta I_{\text{mid}}^k|$  (the change in the orientation of the middle binary due to the kicks, see Equation 9).



**Figure 10.** The survived middle binaries in the  $a_{\text{mid}}^k - e_{\text{mid}}^k$  plane, where  $a_{\text{mid}}^0$  is initialized with different ranges (as labeled).

middle binary with specific  $a_{\text{mid}}^k$  and  $e_{\text{mid}}^k$  can be produced by a wide range of  $(a_{\text{mid}}^0, e_{\text{mid}}^0)$  values.

### 3.3 Constrain the BHB and Tertiary Companion in LK-induced Mergers

Having constrained the range of properties of the middle binary ( $m_{12}$  around  $m_3$ ) following three SNe and the first merger (between  $m_1$  and  $m_2$  leading to  $m_{12}$ ), we now constrain the property of the tertiary  $m_4$  in LK-induced mergers. Based on the result of Section 2.2, the maximum merger fraction in LK-induced mergers is only determined by the properties of the BHB (the middle binary) and is independent of the property of the tertiary companion (see Equation 26). Thus, we can directly identify what kind of BHB systems may have relatively high merger fraction by using Equation (26).

In Figure 11, we show the values of  $f_{\text{merger}}^{\text{max}}$  in the  $a_{\text{mid}} - e_{\text{mid}}$  parameter space, for BHBs with  $m_{12} = 30M_{\odot}$  and  $m_3 = 8M_{\odot}$  (as appropriate for GW190412). We see that almost all the systems with  $a_{\text{mid}}$  less than about 100AU have the merger fraction greater than 1% (dot-dashed line). Higher fractions can be achieved if the BHB is either sufficiently eccentric, or compact (see the contour solid-black line and dashed-black line showing  $f_{\text{merger}}^{\text{max}} = 10\%$ , 5%, respectively). Since the parameter space of the middle binary is also constrained by SNe and kicks (Section 3.2), we consider the systems above the green-dashed line (referring to the survived systems in Figure 9). Thus, all survived systems can potentially have high merger fractions ( $\gtrsim$  a few %) if there is a sufficiently “strong” tertiary companion.

To constrain the parameters of outer binary in our scenario, we pick one representative system with  $a_{\text{mid}} = 15\text{AU}$  and  $e_{\text{mid}} = 0.8$  (see the star symbol shown in Figure 11). The constraints on  $m_4$  and  $a_{\text{out}}$  are shown in Figure 12. In the upper panel, we assume the outer orbit is circular. The orange-dashed line is given by the stability criterion (e.g., Kiseleva et al. 1996), and the orange-solid line corresponds to the weakest tertiary companion ( $\bar{a}_{\text{out,eff}}^{\text{max}}$ ) obtained by Equation (27). We also consider the influence of the merger kick, which happens on  $m_{12}$  and affects the outer binary in an indirect way. This is analogous to the effect on the middle binary due to the natal kick on  $m_1$  (see Section 2.1). In this case, the orbital velocity of the outer binary changes due to the merger kick (cf. Equation 8). By setting the binding energy of the outer binary to zero, we find the boundary where the outer binary remains bound (black line). We see that only a sufficiently massive  $m_4$  can produce GW190412 like events

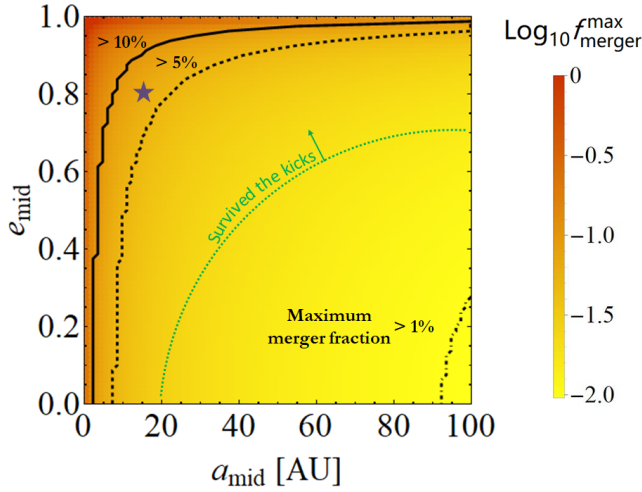


**Figure 11.** The maximum merger fraction of BHBs (the middle binaries) induced by the tertiary companion (Equation 26) in the  $a_{\text{mid}} - e_{\text{mid}}$  parameter plane (this is the same as  $a_{\text{mid}}^k = e_{\text{mid}}^k$  in Figure 9). The binary masses are  $m_{12} = 30M_{\odot}$  and  $m_3 = 8M_{\odot}$  (appropriate for GW190412). The three black lines (solid, dashed and dot dashed) specify  $f_{\text{merger}}^{\text{max}} = 10\%$ ,  $5\%$  and  $1\%$ , respectively. The green-dotted line is from the middle panel of Figure 9, indicating systems that have survived three SNe and kicks.

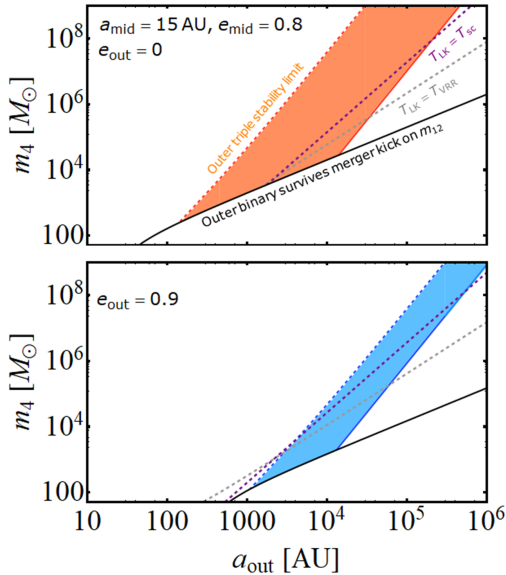


**Figure 12.** Constraints on the mass ( $m_4$ ) and the orbital semi-major axis  $a_{\text{out}}$  of the tertiary companion (MBH) that can lead to LK-induced mergers of the BHB (the middle binary), resembling GW190412. We consider a representative example of the middle binary (with  $a_{\text{mid}} = 15\text{AU}$ ,  $e_{\text{mid}} = 0.8$ ) with a relatively high  $f_{\text{merger}}^{\text{max}}$  (between  $5\%$  and  $10\%$ ; see the star in Figure 11), and include two values of the outer eccentricity:  $e_{\text{out}} = 0$  (upper panel) and  $e_{\text{out}} = 0.9$  (lower panel). The allowed (shaded) regions are constrained by the stability criterion of the outer triple (orange- and blue-dashed lines),  $\bar{a}_{\text{out,eff}}^{\text{max}}$  (orange- and blue-solid lines) and by requiring that the outer binary remains bound in the presence of the merger kick on  $m_{12}$ . The two purple-dashed and gray-dashed lines in each panel indicate the region where the star cluster potential and vector resonant relaxation effect can enhance the BHB merger rate (see Equations 30 and 31).

(color-shaded region in Figure 12). In the lower panel of Figure 12, we consider the case of  $e_{\text{out}} = 0.9$ . We see that the allowed parameter region becomes even more restricted.

If we consider a somewhat different middle binary, e.g.,  $a_{\text{mid}} = 10\text{AU}$ ,  $e_{\text{mid}} = 0.9$ , similar result as Figure 12 can be produced, except that the color-shaded region is slightly shifted to the left side. We therefore conclude that the constraint on  $m_4$ ,  $a_{\text{out}}$  as depicted in Figure 12 is quite representative.

A general conclusion from Figure 12 is that to induce merger of the BHB, the tertiary companion must be at least a few hundreds  $M_{\odot}$ , and falls in the intermediate-mass BH and SMBH regime.

### 3.4 The Effect of Different Natal Kick and Merger Kick

In Sections 3.2 and 3.3, we have assumed that the three stellar-mass BHs all suffered negligible natal kicks. We now examine how larger natal kicks ( $\sigma_{\text{BH}} = 100 \text{ km s}^{-1}$ ) may affect our constraints. We carry out the similar analysis as in Section 3.2, still using the parameters shown in Case I in Table 1, but increase the natal kick velocity when SN explosion occurs. The results are shown in Figure 13. In this case, all four kicks are of order of  $\sim 100 \text{ km s}^{-1}$ . We see that the survival fraction  $f_{\text{survival}}$  is low for all reasonable values of initial  $a_{\text{mid}}^0$ .

We also consider the effect of different values of merger kick (see Figure 14). We evolve the systems with the parameters shown in Case II in Table 1. In this case, both the natal kicks and merger kick are negligible. As a result, almost all the middle binaries we considered can survive with high probabilities, and the survived post-kick  $a_{\text{mid}}^k$  and  $e_{\text{mid}}^k$  cover the whole parameter region (see Figure 14). Of course, in this case, the innermost binary ( $m_1$  and  $m_2$ ) has extreme asymmetric masses (mass ratio = 0.058), which pose question about its formation. Finally, note that the systems from case III in Table 1 have similar behavior as case I, since the merger kick is almost the same in the two cases.

## 4 FORMATION OF GW190814

We now turn our attention to the formation of GW190814 in the “primordial multiple” scenario (see the leftmost pathway in Figure 2). Different from the event GW190412, where the primary component is a merger product, we suggest that the secondary component (mass  $2.6M_{\odot}$ ) in GW190814 is the remanet from a previous merger of two NSs (see Figure 15). Since the spin parameter of the secondary in GW190814 is not constrained from the GW data, we cannot constrain the mass ratio ( $m_2/m_1$ ) as in the case of GW190412 (Section 3.1). Instead, we assume that the  $2.6M_{\odot}$  secondary results from the merger of two  $1.4M_{\odot}$  NSs, and each NS has evolved from a Helium star of mass  $4M_{\odot}$ . The SN explosion leads to significant mass ejection, accompanied by a large natal kick ( $\sigma_{\text{NS}} = 260 \text{ km s}^{-1}$ ).

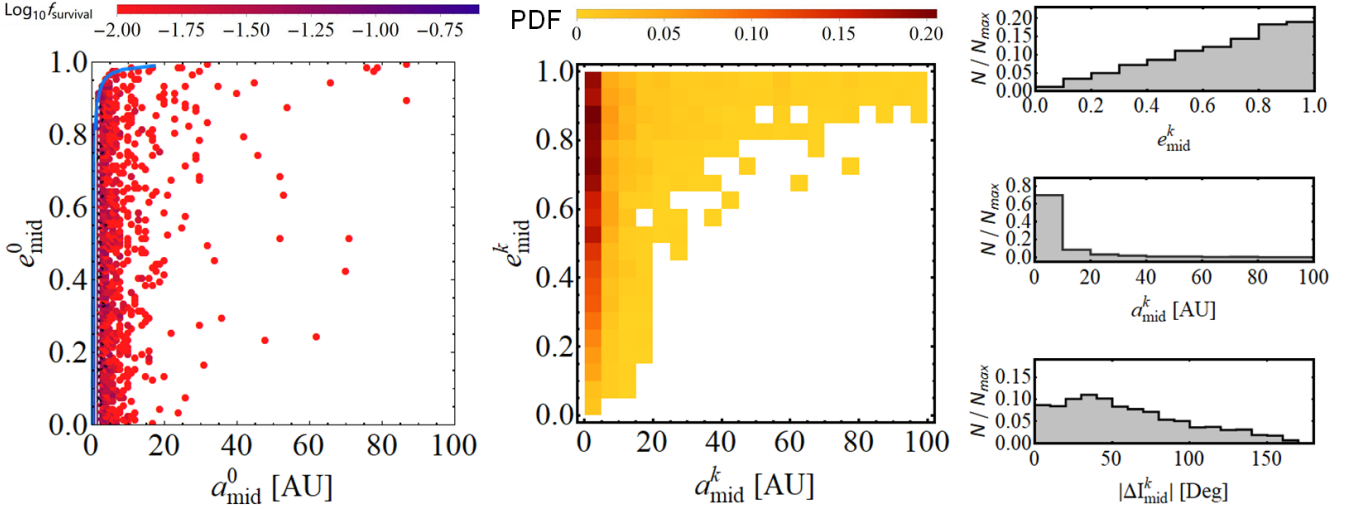


**Figure 13.** Similar to Figure 9, but with a larger natal kick for BH formation ( $\sigma_{\text{BH}} = 100 \text{ km s}^{-1}$ ).

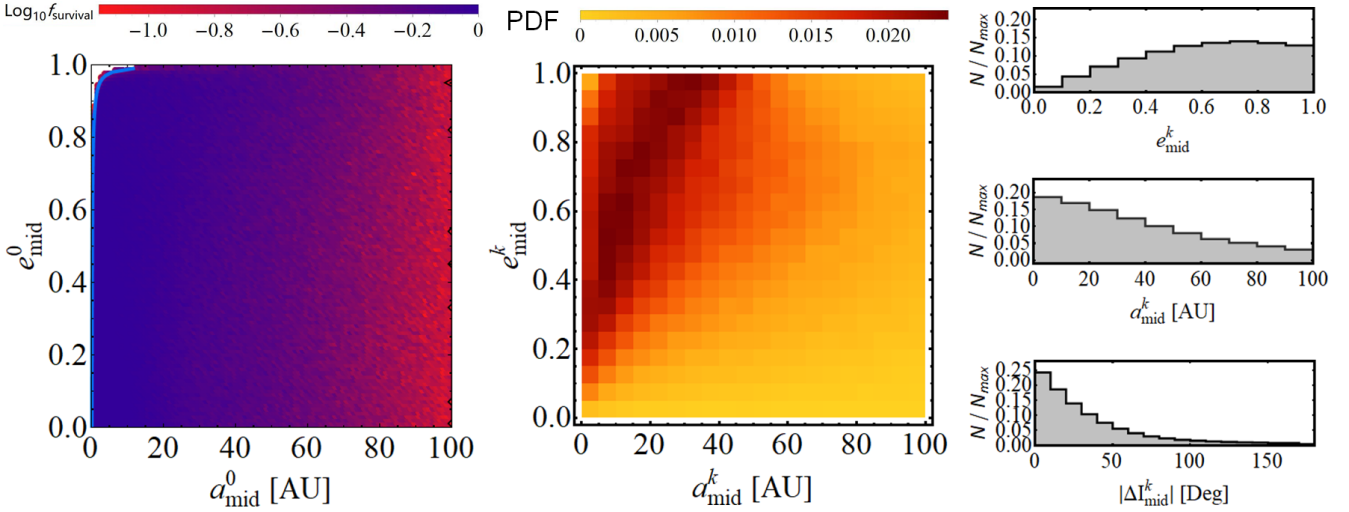


**Figure 14.** Same as Figure 9, but with small merger kick of  $V_{\text{mk}} = 27.1 \text{ km s}^{-1}$  (see Case II in Table 1).

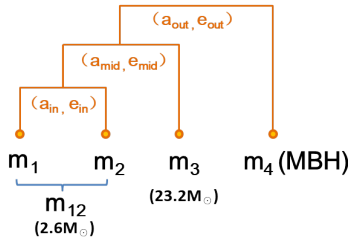


**Figure 15.** Schematic diagram of a hierarchical quadruple system for forming GW190814, where the secondary component (mass  $2.6 M_{\odot}$ ) is a merger remnant of two NSs.

To produce GW190814-like BHBs in our scenario, we evolve the inner triple systems (see Figure 15) that undergo three natal kicks and one merger kick. Different from GW190412, the first SN occurs on  $m_3$ , which is the most massive component. We set the natal kick on this BH to

zero. Then, the other two progenitors experience SN explosions and the newly born NSs receive significant natal kicks. Over time, the binary NSs merge by themselves. The merger kick received on the remnant is negligible because  $m_1 = m_2$  (see Figure 7).

Following the same strategy as described in Section 3.2, we obtain the orbital distributions of the survived middle binaries. The results are shown in Figure 16. The left panel presents the pre-kick distributions of  $a_{\text{mid}}^0$  and  $e_{\text{mid}}^0$ . The systems enclosed by the solid-blue line are stable, where we set  $a_{\text{in}}^0 = 0.1 \text{ AU}$  and  $e_{\text{in}}^0 = 0$  for the inner binary (e.g., Belczynski et al. 2018). Note that unlike the case of GW190412, the distributions of  $a_{\text{mid}}^0$  and  $e_{\text{mid}}^0$  for the survived systems depend on the  $a_{\text{in}}^0$  and  $e_{\text{in}}^0$  sensitively: e.g., if we choose  $a_{\text{in}}^0 = 0.14 \text{ AU}$ , the number of survived systems can decrease by over 90%. This results from the fact that a large natal kick on the NS can easily destroy the systems and some of



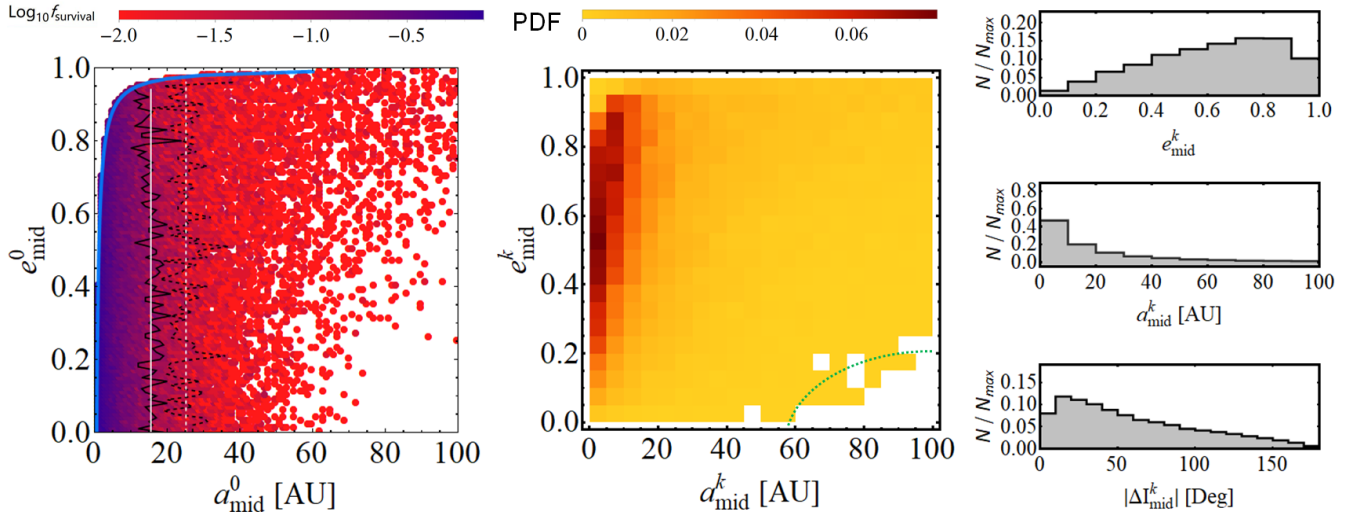


**Figure 16.** Similar to Figure 9, but for the systems that lead to GW190814-like binaries. In this calculation, the pre-SN component masses are  $m_1^0 = m_2^0 = 4M_\odot$  and  $m_3^0 = 25.8M_\odot$ , and post-SN masses are  $m_1^k = m_2^k = 1.4M_\odot$  and  $m_3^k = 23.2M_\odot$ . In the inner binary, each newly formed NS receives a large natal kick ( $\sigma_{\text{NS}} = 260\text{km s}^{-1}$ ) during the SN explosion. For the post-SN BH, we assume  $\sigma_{\text{BH}} = 0\text{km s}^{-1}$ . The merger of  $m_1^k$  and  $m_2^k$  leads to the remnant with mass  $m_{12} = 2.6M_\odot$  and with negligible merger kick.

the remaining NS binaries cannot merge within a Hubble times. Similar to Figure 9, the middle and right panels of Figure 16 show the post-kick distributions of  $a_{\text{mid}}^k$  and  $e_{\text{mid}}^k$ . We see that the systems that survived the kicks can cover near the whole parameter space in the middle panel. If the natal kick for the newly formed BH ( $m_3$ ) is increased to  $\sigma_{\text{BH}} = 100\text{km s}^{-1}$ , a significant reduction of survivals can be found, similar to the case depicted in Figure 13.

To determine the merger fractions of the middle binaries, we carry out calculations similar to the one in Section 3.3. The results are shown in Figure 17. We find that compared to the example in Figure 11, the parameter region with high merger fraction ( $f_{\text{merger}}^{\text{max}} \gtrsim 10\%$ ,  $5\%$ ) is narrower. This is because the component masses of the middle binary ( $m_{12} = 2.6M_\odot$  and  $m_3 = 23.2M_\odot$ ) are smaller, GW radiation becomes less efficient, reducing the number of systems which are able to merge within a Hubble time.

In Figure 18, we show the constrained parameter space for the tertiary companion  $m_4$  (MBH), where we consider the representative middle binary orbital parameters  $a_{\text{mid}} = 12\text{AU}$  and  $e_{\text{mid}} = 0.85$  (see the star symbol shown in Figure 17). Different from the case of GW190412, the middle binary here is affected by the large natal kicks on  $m_1$  or  $m_2$  (instead of the merger kick on  $m_{12}$ ), and varying the middle binary property can influence the constraint on the outer binary. Nevertheless, we see from Figure 18 that in general, a large tertiary mass (from  $100M_\odot$  to  $\gtrsim 10^8M_\odot$ ) is required to induce merger of the GW190814-like BHBs.

## 5 FORMATION OF GW190521

Since the two BHs in GW190521 likely fall in the high mass gap, and each BH has a dimensionless spin parameter close to  $\sim 0.7$ , we suggest that both the components

in this source are 2G BHs and are produced by previous equal-mass mergers (see Figure 7). Therefore, in our “primordial” multiple scenario (see the left pathway in Figure 3), we consider a quadruple system consisting of two inner binaries, and the progenitor masses are  $(47.2M_\odot, 47.2M_\odot)$  and  $(36.7M_\odot, 36.7M_\odot)$ . We assume that the system goes through SN explosion on each component with a negligible natal kick ( $\sigma_{\text{BH}} = 0\text{km s}^{-1}$ ) and sudden mass loss, as well as two merger kicks with  $V_{\text{mk}} \simeq 0\text{km s}^{-1}$  (because of the equal-mass merger; see Figure 7). Eventually, the two remnants form the middle binary, which then merge with the aid of an external companion  $m_5$  (the MBH; see Figure 3).

For the survival fraction of the middle binaries, different from GW190412 and GW190814, all kicks are negligible in the case of GW190521. Thus, we expect that almost all the middle binaries satisfying the stability criterion can survive with high probabilities. The distribution of the post-kick  $a_{\text{mid}}^k$  and  $e_{\text{mid}}^k$  is expected to be similar to Figure 14 (since Figure 14 also corresponds to the case with small natal kick and merger kick).

For the merger fractions, we use the same approach as in Section 3.3 and present the results in Figure 19. Since the component masses of the middle binary are large ( $85M_\odot$  and  $66M_\odot$ ), we find that the parameter region with  $f_{\text{merger}}^{\text{max}} \gtrsim 10\%$  ( $5\%$ ) are the broader compared to the other examples in Figures 11 and 17.

We show the constrained parameters for the external companion (i.e., the fifth body  $m_5$ , the MBH) in Figure 20. Here, we consider the representative middle binary orbital parameters  $a_{\text{mid}} = 15\text{AU}$  and  $e_{\text{mid}} = 0.8$  (see the star symbol shown in Figure 19). Note that in this case, there are no constraints on  $m_5$  and  $a_{\text{out}}$  from the natal kick and merger kick. Again, we find that a broad range of  $m_5$  values are possible.



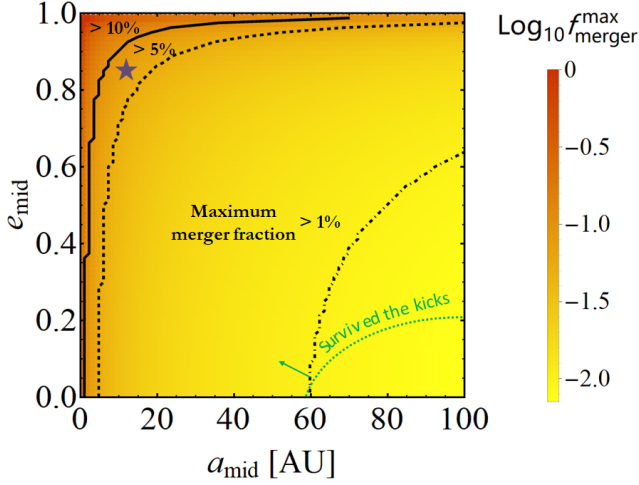


**Figure 17.** Similar to Figure 11, but for the middle binary with  $m_{12} = 2.6M_{\odot}$ , and  $m_3 = 23.2M_{\odot}$  (appropriate for GW190814-like events). The green dashed line is the same as the one in the middle panel of Figure 16.

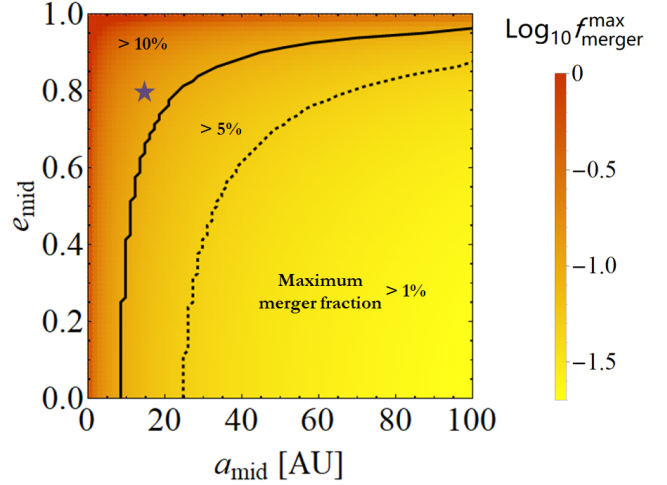


**Figure 19.** Similar to Figure 11, but for the middle binary with  $m_{12} = 85M_{\odot}$ , and  $m_3 = 66M_{\odot}$  (appropriate for GW190521-like events). Since both the natal kick and merger kick are negligible, all  $(a_{\text{mid}}, e_{\text{mid}})$  values can survive the kicks.

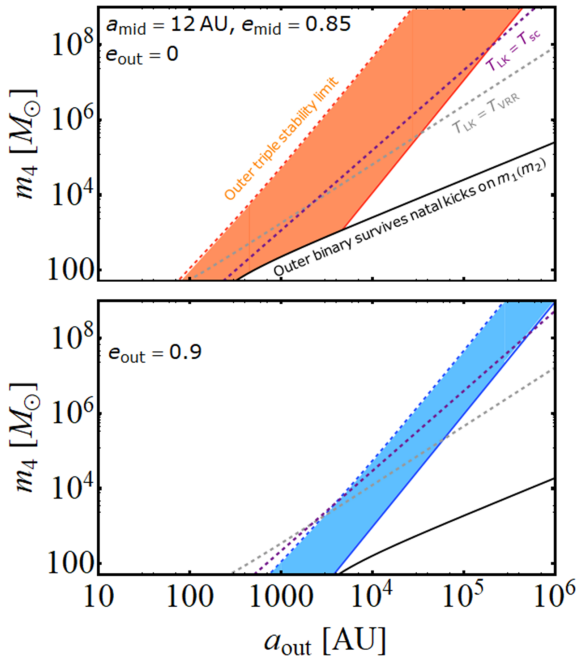


**Figure 18.** Similar to Figure 12, but for GW190812-like events. The representative middle binary has  $m_{12} = 2.6M_{\odot}$ ,  $m_3 = 23.2M_{\odot}$ ,  $a_{\text{mid}} = 12\text{AU}$  and  $e_{\text{mid}} = 0.85$ .

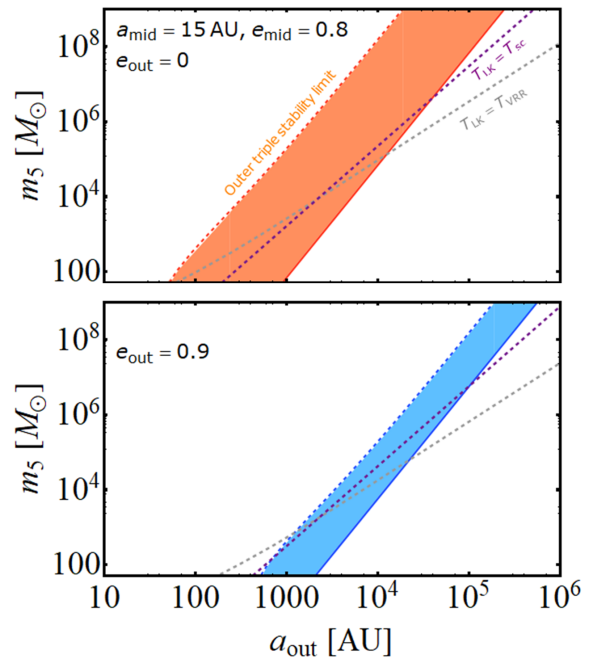


**Figure 20.** Similar to Figure 12, but for GW190521-like events. The representative middle binary has  $m_{12} = 85M_{\odot}$ ,  $m_3 = 66M_{\odot}$ ,  $a_{\text{mid}} = 15\text{AU}$  and  $e_{\text{mid}} = 0.8$ . Note that since the kicks are negligible, there are no constraints from kicks on the tertiary companion.

## 6 DYNAMICALLY FORMED BH BINARIES

In Sections 3-5 we have studied in detail the formation of GW190412, GW190814 and GW190521-like systems assuming that the BHBs (the middle binary in Figure 4) are produced in “primordial” multiple systems (the leftmost pathway in Figures 1-3). As noted in Section 1, these BHBs can also form dynamically, especially when the external companion is a SMBH. Indeed, the kinds of systems we study may be naturally found in the nuclear star cluster around

a SMBH. Recent studies show that hierarchical systems of stars and compact remnants can form through few-body encounters in dense star clusters, either through binary-single interaction (e.g., Samsing et al. 2014) or through binary-binary interaction (e.g., Fragione et al. 2020).

Suppose the BHBs leading to the three LIGO/VIRGO events could be assembled dynamically in nuclear star clusters, the masses of their progenitor systems are constrained

by two factors: (i) In typical binary-single (or binary) encounters, a single (or a tight binary) is exchanged into a bound orbit, while the lightest mass is ejected; (ii) If a binary component is a merger remnant and its mass and spin are known from the GW data (as in the case of GW190412), then the masses of its progenitors can be constrained (see Section 3.1).

Figures 1-3 show the possible dynamical pathways leading to the formation of BHBs in the three LIGO/VIRGO O3 events. Taking the GW190412 as an example (Figure 1), a compact BHB with mass ( $25.2M_{\odot}$ ,  $5.3M_{\odot}$ ) or ( $21.9M_{\odot}$ ,  $9.2M_{\odot}$ ) (see Case I and III in Table 1) merges first. Then, the newly form (2G) BH interacts with a binary ( $8M_{\odot}$ ,  $4M_{\odot}$ ), leaving behind a BHB with mass ( $30M_{\odot}$ ,  $8M_{\odot}$ ) and an escaper  $4M_{\odot}$ . Alternatively, the compact ( $25.2M_{\odot}$ ,  $5.3M_{\odot}$ ) or ( $21.9M_{\odot}$ ,  $9.2M_{\odot}$ ) binary may experience a close encounter with the wide ( $8M_{\odot}$ ,  $4M_{\odot}$ ) binary first, replacing the light component in the wide binary. Then, the compact binary in this triple can merge (either by itself, or through LK oscillations), leading to the 2G BH ( $30M_{\odot}$ ). Eventually the GW190412-like “middle” binary is formed.

Numerous uncertainties exist in these dynamical scenarios, including the formation fraction and survival fraction of the BHBs (the middle binaries). The former depends on the density, initial mass function and binary abundance in the cluster. The latter is mostly determined by the merger kick (received by the 2G BH), since a large fraction of the dynamically formed triple/binary population consists of BHs (e.g., Fragione et al. 2020). These uncertainties imply that the distributions of the survived middle binaries in  $a_{\text{mid}}^k - e_{\text{mid}}^k$  parameter plane are highly uncertain.

Nevertheless, we expect that a broad range of  $a_{\text{mid}}$  and  $e_{\text{mid}}$  can be produced dynamically. The merger fractions shown in Figures 11, 17 and 19 still apply to the dynamically formed BHBs, except that the green “survived kicks” lines in Figures 11 and 17 are irrelevant. Similarly, Figures 12, 18, 20 are still valid for dynamically formed BHBs, except that the “outer binary survives merger (natal) kick” lines in Figures 12 and 18 are irrelevant. Overall, these figures provide constraints on the masses of the MBH and the locations where tertiary-induced mergers can happen leading to these three LIGO/VIRGO events.

## 7 DISCUSSION

### 7.1 How common are GW190412, GW190814 and GW190521-like events?

The main goal of this paper is to constrain what kinds of binary/triple/quadrupole systems (e.g. the range of  $a_{\text{mid}}$  and  $m_{\text{MBH}}$ ) can lead to GW190412, GW190814 and GW190521-like events in the hierarchical tertiary-induced merger scenario. Given the uncertainties in the binary/triple/quadrupole populations (especially those in dense star clusters), a systematical evaluation of the occurrence rates of such events is beyond the scope of this paper

— our calculations presented in previous sections were not set up for population synthesis study. Indeed, our view is that full population synthesis study (starting from main sequence stellar binaries and triples) would involve too many uncertainties to be valuable at this point. Nevertheless, it is of interest to have a crude, back-of-the-envelope estimates of the merger rates for GW190412, GW190814 and GW190521-like events in our scenario. We carry out such estimate in the following. Since we do not consider full stellar evolution (except SNe and natal kicks) in our study, we evaluate the merger rate of these 2G BHs using the merger rate ( $\mathcal{R}_{1\text{G}}$ ) of 1G BHs (or NSs in the case GW190814), which we assume to be a fraction of the detection rate of “normal” BH or NS mergers from LIGO/VIRGO O1-O2 runs. Although our analysis in Sections 3-5 are quite general, the results indicate that the tertiary companion is likely a MBH. We therefore envision that these events likely take place in dense star clusters around MBHs.

A key uncertainty in our rate estimate is the “primordial” stellar or BH multiplicity. It is shown observationally that the majority of massive stars are born in binaries or higher-order multiple systems (e.g., Sana et al. 2012). The situation in nuclear star clusters is unclear, but we expect that even higher multiple fractions are possible. We assume that the formation fraction of stellar triples  $f_{\text{triple}}$  is about 50%.

First consider the GW190412-like events (see Figure 1 or 4). The BHBs (middle binaries) in our simulations can have significant survival fraction and merger fraction, i.e.,  $f_{\text{survival}}, f_{\text{merger}} \gtrsim 10\%$ , when the BH natal kicks are negligible (see Sections 3.2 and 3.3). Therefore, the merger rate of 2G BHs can be estimated as <sup>4</sup>:

$$\begin{aligned} \mathcal{R}_{2\text{G}} &= \mathcal{R}_{1\text{G}} \times f_{\text{triple}} \times f_{\text{survival}} \times f_{\text{merger}} \\ &\sim \mathcal{R}_{1\text{G}} \times 50\% \times 10\% \times 10\% \\ &\simeq 0.5\% \times \mathcal{R}_{1\text{G}}. \end{aligned} \quad (28)$$

If we take the merger rate of 1G BHs in our scenario,  $\mathcal{R}_{1\text{G}}$ , to be fraction of the LIGO O1-O2 detection rate,  $\mathcal{R}_{\text{obs}} = 10 - 100 \text{ Gpc}^{-3} \text{ yr}^{-1}$  (Abbott et al. 2019a), we find  $\mathcal{R}_{2\text{G}} \lesssim 0.05 - 0.5 \text{ Gpc}^{-3} \text{ yr}^{-1}$ . Note that  $\mathcal{R}_{2\text{G}}$  will be lower if the natal kicks on the BHs are significant, as the binary survival fraction will be decreased. On the other hand, various “environmental” effects may increase the merger fraction  $f_{\text{merger}}$  by a factor of a few (see Section 7.2). For reference, Abbott et al. (2020a) suggested that the merger rate

<sup>4</sup> Note that in Equation (28), we have adopted  $f_{\text{survival}} \sim 10\%$  based on our canonical calculation in Section 3.2 (see Figure 9). If the triple population contains systems with  $a_{\text{mid}}^0$  beyond 100 AU,  $f_{\text{survival}}$  would be reduced by a factor of  $\sim 2$  (note that the  $a_{\text{mid}}^0$  distribution of stellar binaries beyond 100 AU is steeper than  $(a_{\text{mid}}^0)^{-1.5}$ ; see Moe & Di Stefano 2017; El-Badry & Rix 2018; Tian et al. 2020). On the other hand, if the triple population in dense star cluster favors systems with  $a_{\text{mid}}^0$  much smaller than 100 AU,  $f_{\text{survival}}$  could be increased somewhat. In any case, what matter is the product  $f_{\text{triple}} \times f_{\text{survival}}$ , which we have taken to be 5% in Equation (28).

of BHBs with mass ratio  $m_2/m_1 \lesssim 0.4$  is about 10% of the O1-O2 rate, i.e.,  $1 - 10 \text{ Gpc}^{-3} \text{ yr}^{-1}$ , and the rate for BHB mergers with  $m_2/m_1 \lesssim 0.25$  (like GW190412) is even lower (see also [Olejak et al. 2020](#)). Our upper limit for  $\mathcal{R}_{2G}$  for GW190412-like events is nominally smaller than the “observed” LIGO rate, but given the various uncertainties, it could also be consistent with the LIGO rate.

For the GW190814-like events (see Figure 2), we again set  $f_{\text{survival}}, f_{\text{merger}} \simeq 10\%$  and obtain  $\mathcal{R}_{2G} \sim 0.5\% \times \mathcal{R}_{1G}$ . The observed rate of 1G NS binaries suggested by LIGO is about  $\mathcal{R}_{\text{obs}} = 250 - 2810 \text{ Gpc}^{-3} \text{ yr}^{-1}$  (e.g., [Abbott et al. 2020b](#)), so our inferred merger rate induced by a tertiary is  $\mathcal{R}_{2G} \lesssim 1 - 14 \text{ Gpc}^{-3} \text{ yr}^{-1}$ . We emphasize that this rate estimate is highly uncertain since the survival fraction depends sensitively on the initial configuration of the system, where the large natal kicks on newly born NSs can destroy the “middle” binaries. For reference, the LIGO detection rate of GW190814-like events is about  $\sim 1 - 23 \text{ Gpc}^{-3} \text{ yr}^{-1}$  ([Abbott et al. 2020c](#)), and our estimate for  $\mathcal{R}_{2G}$  is consistent with this “observed” value.

For the GW190521-like binaries (see Figure 3), the survival fraction and merger fraction can be higher compared to the other sources if we adopt negligible natal kick and merger kick (see Section 5). Assuming an upper limit  $f_{\text{survival}} \simeq 60\%$  and  $f_{\text{merger}} \simeq 20\%$  (based on the discussion in Section 5), we find  $\mathcal{R}_{2G} \sim 6\% \times \mathcal{R}_{1G}$ . Using  $\mathcal{R}_{1G} \lesssim 10 - 100 \text{ Gpc}^{-3} \text{ yr}^{-1}$ , we find  $\mathcal{R}_{2G} \lesssim 0.6 - 6 \text{ Gpc}^{-3} \text{ yr}^{-1}$ . Note that this is an optimistic estimate: The survival fraction can be lower if the binary components come from the mergers of BHB with highly asymmetric masses (i.e., merger kick can be large). For reference, the merger rate given by LIGO/VIRGO for GW190521-like events is  $\sim 0.02 - 0.43 \text{ Gpc}^{-3} \text{ yr}^{-1}$  ([Abbott et al. 2020d](#)).

Overall, although the above estimates indicate that the rate for tertiary-induced mergers in multiples could be consistent with the LIGO/VIRGO findings, our estimates could be too optimistic. The merger rate of 1G BHs near the MBH/SMBH is quite uncertain. Also, the survival fraction can be lower if the natal kick of newly born BH is large, leading to smaller merger rate estimates.

## 7.2 “Environmental” Effects

Our analyses in Sections 3-5 do not take into account the effects related to dense stellar environment. Since we have found that the external companion in our scenario is likely a MBH, the effects from the cluster may play an important role and change the configurations of the inner triple systems studied here. We list three main effects as follows.

In a dense stellar environment, the BHB (the middle binary) may be perturbed through multiple encounters with other passing objects. The orbital parameters may change significantly, leading to binary evaporation. The typical timescale can be estimated as (e.g., [Binney & Tremaine](#)

1987)

$$T_{\text{evap}} = \frac{(m_{12} + m_3)\sigma_{\text{cl}}}{16\sqrt{\pi}Ga_{\text{mid}}\langle m \rangle\rho_{\text{cl}}\ln\Lambda}. \quad (29)$$

To evaluate  $T_{\text{evap}}$ , we assume the stellar velocity dispersion  $\sigma_{\text{cl}} = 280 \text{ km s}^{-1} \sqrt{0.1 \text{ pc}/a_{\text{out}}}$  (e.g., [Kocsis & Tremaine 2011](#)), the stellar density  $\rho_{\text{cl}} = 0.8 \times 10^5 m_{\odot} \text{ pc}^{-3} (a_{\text{out}}/\text{pc})^{-1.3}$  (appropriate for Milky Way galactic center; [Fritz et al. 2016](#)), the averaged stellar mass in the cluster  $\langle m \rangle = 1 M_{\odot}$ , and the Coulomb logarithm  $\ln\Lambda \simeq 2$ . In the examples of Figures 12, 18 and 20, we find that  $T_{\text{evap}}$  is always greater than the LK timescale  $T_{\text{LK}}$  if  $a_{\text{out}} \lesssim 10^6 \text{ AU}$ <sup>5</sup>. Therefore, the MBH can induce LK merger of the middle binary before the disruption of middle binary (color-shaded region).

Another effect is resonant relaxation, which affects orbits close to the MBH, and changes both the magnitude and direction of the orbital angular momentum (e.g., [Rauch & Tremaine 1996](#)). The timescale for the relaxation of the orbital orientation vectors (the “Vector Resonant Relaxation”, or VRR) is given by (e.g., [Hamers et al. 2018](#))

$$T_{\text{VRR}} = \frac{P_{\text{out}}}{\beta} \frac{m_{\text{MBH}}}{\sqrt{N_{\text{cl}}}}, \quad (30)$$

where  $\beta \sim 2$ ,  $P_{\text{out}}$  is the orbital period of the outer binary,  $N_{\text{cl}}$  is the number of stars within radius  $r = a_{\text{out}}$  from the MBH. Because VRR can change the orientation of BHB+SMBH binary orbit, it can enhance the tertiary-induced merger rate by opening up the LK window through an “inclination resonance” (e.g., [Hamers & Lai 2017](#); [Hamers et al. 2018](#)), provided that  $T_{\text{VRR}}$  is less than  $T_{\text{LK}}$ . The grey dashed lines in Figures 12, 18 and 20 indicate  $T_{\text{VRR}} = T_{\text{LK}}$ , highlighting the systems that might have such “inclination resonance”.

Finally, if the nuclear star cluster has a non-spherical mass distributions, the BHB’s orbit around the central MBH will experience nodal precession induced by the non-spherical cluster potential. The characteristic timescale is (e.g., [Petrovich & Antonini 2017](#))

$$T_{\text{sc}} = \frac{1}{\epsilon_z G P_{\text{out}} \rho_{\text{cl}}}, \quad (31)$$

where  $\epsilon_z$  is dimensionless and measures the asphericity of the cluster mass distribution. Thus, for a BHB embedded in such environment, the angular momentum of the orbit around the MBH may vary in time, changing the inclination angle between the inner and outer orbits. When the precession time  $T_{\text{sc}}$  is comparable to the LK timescale  $T_{\text{LK}}$ , the merger window of the BHB induced by the SMBH can increase as a result of the “inclination resonance”, further enhancing the BHB merger rate ([Petrovich & Antonini 2017](#)). The “ $T_{\text{sc}} = T_{\text{LK}}$ ” lines (assuming  $\epsilon_z \sim 0.1$ ) in Figures 12, 18

<sup>5</sup> Here, we only consider one example of the galactic center, and do not take into account the possible dependence of  $\sigma_{\text{cl}}$  and  $\rho_{\text{cl}}$  on  $m_4$  (that is complicated and highly uncertain). In some of the nuclear star cluster,  $T_{\text{evap}}$  could be short and BHBs may not survive for a sufficiently long time.

and 20 indicate the systems for which such enhancements are effective.

Overall, these dynamical effects of the cluster environment can increase the merger fraction of BHBs induced by the SMBH from 10% to more than 30–50%, thus increasing our rate estimates in Section 7.1 by a factor of a few.

## 8 SUMMARY

We have studied the formation of three exceptional LIGO/VIRGO O3 events, GW190412, GW190814 and GW190521, in hierarchical multiple systems, where one or both components of the binary come from a previous merger. In our scenario, the multiples could be either “primordial” or formed dynamically in dense stellar clusters (see Figures 1-3). Regardless of the detailed evolutionary pathways, the final black-hole binaries (BHBs) generally have too wide orbital separations to merge by themselves. Instead, with the aid of an external companion (likely a massive black hole, MBH), the binary can merge over the cosmic time due to Lidov-Kozai (LK) eccentricity oscillations. During its evolution, the progenitor multiple system undergoes supernova explosions to form BHs or NSs accompanied by mass losses and natal kicks, and may also experience kick when the first-generation BHs merge. All these kicks and mass losses can change the configuration/geometry of the hierarchical multiple, or even break up the system. We explore the binaries that are most likely to survive the kicks, and use the post-kick binary distributions to constrain the parameter space of the external companion which can give rise to LK-induced BHB mergers.

The results of our calculations can be summarized as follows.

(i) For the inner triple systems in our “primordial” multiple scenario (Figure 4; see also the leftmost pathway in Figures 1-3), only the relative compact middle binaries can survive both natal and merger kicks, even though the natal kick on a newly born BH may be negligible (see the left panels of Figures 9 and 16). The distributions of the post-kick orbital parameters of all survivals show that the majority of systems have either small semimajor axes or large eccentricities (see the middle and right panels of Figures 9 and 16). This is partly because the wide binaries can be easily destroyed and partly because the sudden mass loss can increase the orbital eccentricity.

(ii) For the LK-induced BHB mergers with sufficiently massive tertiary (such as MBH), the octupole effects are negligible, and the merger fraction (assuming the orientation of the tertiary is isotropically distributed) as a function of the binary and tertiary parameters can be determined analytically (Section 2.2, Figure 5). The maximum merger fraction ( $f_{\text{merger}}^{\text{max}}$ ) is given by the analytical formula (26). The value of  $f_{\text{merger}}^{\text{max}}$  depends only on the properties of the BHB, instead of the tertiary companion. The strength of the tertiary perturbation can be characterized by the dimensionless effective semi-major axis  $\bar{a}_{\text{out,eff}}$  (see Equation 25). The weakest per-

turbation (the largest  $\bar{a}_{\text{out,eff}}$ ), beyond which no merger can occur, is given by the analytical formula (27).

(iii) Based on the systems that have survived SNe and kicks, together with our analytical formulae for LK-induced mergers, we constrain the properties of the tertiary companions required to produce the three LIGO/VIRGO O3 events (see Figures 12, 18 and 20). These constraints indicate that the tertiary companions must be at least a few hundreds  $M_{\odot}$ , and fall in the intermediate-mass BH and supermassive BH range.

(iv) Based on our calculations, we suggest that GW190412, GW190814 and GW190521 could all be produced via hierarchical mergers in multiples: Through different evolutionary pathways (Figures 1-3), a BHB is assembled, likely in a dense nuclear star cluster, and the final merger is induced by a MBH or SMBH. We estimate the event rates of such hierarchical mergers based on the “normal” BHB or NS binary merger rates from LIGO/VIRGO O1-O2 runs and our calculated binary survival and merger fractions. The merger rate given by this tertiary-induced channel is very uncertain. But our optimistic estimate indicates that the rate could be consistent with the LIGO/VIRGO findings (Section 7.1).

## 9 ACKNOWLEDGMENTS

This work is supported in part by the NSF grant AST-1715246.

## 10 DATA AVAILABILITY

The simulation data underlying this article will be shared on reasonable request to the corresponding author.

## REFERENCES

- Abbott B. P., Abbott R., Abbott T. D., Abraham S., Acernese F., Ackley K., Adams C., et al., 2019, *PhRvX*, 9, 031040
- Abbott B. P., Abbott R., Abbott T. D., Abraham S., Acernese F., Ackley K., Adams C., et al., 2019, *ApJL*, 882, L24
- Abbott R., Abbott T. D., Abraham S., Acernese F., Ackley K., Adams C., Adhikari R. X., et al., 2020, *PhRvD*, 102, 043015
- Abbott B. P., Abbott R., Abbott T. D., Abraham S., Acernese F., Ackley K., Adams C., et al., 2020, *ApJL*, 892, L3
- Abbott R., Abbott T. D., Abraham S., Acernese F., Ackley K., Adams C., Adhikari R. X., et al., 2020, *ApJL*, 896, L44
- Abbott R., Abbott T. D., Abraham S., Acernese F., Ackley K., Adams C., Adhikari R. X., et al., 2020, *PhRvL*, 125, 101102
- Abbott R., Abbott T. D., Abraham S., Acernese F., Ackley K., Adams C., Adhikari R. X., et al., 2020, *ApJL*, 900, L13



- Anderson K. R., Storch N. I., Lai D., 2016, *MNRAS*, 456, 3671
- Anderson K. R., Lai D., Storch N. I., 2017, *MNRAS*, 467, 3066
- Antonini F., Perets H. B., 2012, *ApJ*, 757, 27
- Antonini F., Toonen S., Hamers A. S., 2017, *ApJ*, 841, 77
- Bailyn C. D., Jain R. K., Coppi P., Orosz J. A., 1998, *ApJ*, 499, 367
- Banerjee S., Baumgardt H., Kroupa P., 2010, *MNRAS*, 402, 371
- Barkat Z., Rakavy G., Sack N., 1967, *PhRvL*, 18, 379
- Bartos I., Kocsis B., Haiman Z., Márka S., 2017, *ApJ*, 835, 165
- Belczynski K., Dominik M., Bulik T., O’Shaughnessy R., Fryer C., Holz D. E., 2010, *ApJ*, 715, L138
- Belczynski K., Holz D. E., Bulik T., O’Shaughnessy R., 2016, *Natur*, 534, 512
- Belczynski K., Askar A., Arca-Sedda M., Chruslinska M., Donnari M., Giersz M., Benacquista M., et al., 2018, *A&A*, 615, A91
- Binney J., Tremaine S., 1987, *gady.book*
- Blaes O., Lee M. H., Socrates A., 2002, *ApJ*, 578, 775
- Gerosa D., Vitale S., Berti E., 2020, *PhRvL*, 125, 101103
- Di Carlo U. N., Mapelli M., Giacobbo N., Spera M., Bouffanais Y., Rastello S., Santoliquido F., et al., 2020, *arXiv*, [arXiv:2004.09525](https://arxiv.org/abs/2004.09525)
- Downing J. M. B., Benacquista M. J., Giersz M., Spurzem R., 2010, *MNRAS*, 407, 1946
- Dominik M., Belczynski K., Fryer C., Holz D. E., Berti E., Bulik T., Mandel I., O’Shaughnessy R., 2012, *ApJ*, 759, 52
- Dominik M., Belczynski K., Fryer C., Holz D. E., Berti E., Bulik T., Mandel I., O’Shaughnessy R., 2013, *ApJ*, 779, 72
- Dominik M., et al., 2015, *ApJ*, 806, 263
- El-Badry K., Rix H.-W., 2018, *MNRAS*, 480, 4884
- Fabrycky D., Tremaine S., 2007, *ApJ*, 669, 1298
- Farr W. M., Sravan N., Cantrell A., Kreidberg L., Bailyn C. D., Mandel I., Kalogera V., 2011, *ApJ*, 741, 103
- Ford E. B., Kozinsky B., Rasio F. A., 2000b, *ApJ*, 535, 385
- Fragione G., Kocsis B., 2019, *MNRAS*, 486, 4781
- Fragione G., Loeb A., 2019, *MNRAS*, 486, 4443
- Fragione G., Loeb A., 2019, *MNRAS*, 490, 4991
- Fragione G., Martinez M. A. S., Kremer K., Chatterjee S., Rodriguez C. L., Ye C. S., Weatherford N. C., et al., 2020, *arXiv*:2007.11605
- Fritz T. K., Chatzopoulos S., Gerhard O., Gillessen S., Genzel R., Pfuhl O., Tacchella S., et al., 2016, *ApJ*, 821, 44
- Fuller J., Piro A. L., Jermyn A. S., 2019, *MNRAS*, 485, 3661
- Fuller J., Ma L., 2019, *ApJL*, 881, L1
- Hamers A. S., Lai D., 2017, *MNRAS*, 470, 1657
- Hamers A. S., Bar-Or B., Petrovich C., Antonini F., 2018, *ApJ*, 865, 2
- Hamers A. S., Safarzadeh M., 2020, *arXiv*, [arXiv:2005.03045](https://arxiv.org/abs/2005.03045)
- Hoang B.-M., Naoz S., Kocsis B., Rasio F. A., Dosopoulou F., 2018, *ApJ*, 856, 140
- Hobbs G., Lorimer D. R., Lyne A. G., Kramer M., 2005, *MNRAS*, 360, 974
- Kocsis B., Tremaine S., 2011, *MNRAS*, 412, 187
- Kozai Y., 1962, *AJ*, 67, 591
- Kiseleva L. G., Aarseth S. J., Eggleton P. P., de La Fuente Marcos R., 1996, *ASPC*, 90, 433
- Lidov M. L., 1962, *Planet. Space Sci.*, 9, 719
- Lipunov V. M., Postnov K. A., Prokhorov M. E., 1997, *AstL*, 23, 492
- Lipunov V. M., et al., 2017, *MNRAS*, 465, 3656
- Liu B., Muñoz D. J., Lai D., 2015, *MNRAS*, 447, 747
- Liu B., Lai D., 2018, *ApJ*, 863, 68
- Liu B., Lai D., 2019, *MNRAS*, 483, 4060
- Liu B., Lai D., Wang Y.-H., 2019, *ApJ*, 881, 41
- Liu B., Lai D., Wang Y.-H., 2019, *ApJL*, 883, L7
- Liu B., Lai D., 2020, *PhRvD*, 102, 023020
- Lousto C. O., Campanelli M., Zlochower Y., Nakano H., 2010, *CQGra*, 27, 114006
- Lu W., Beniamini P., Bonnerot C., 2021, *MNRAS*, 500, 1817
- Mandel I., 2016, *MNRAS*, 456, 578
- Mandel I., de Mink S. E., 2016, *MNRAS*, 458, 2634
- Mandel I., Fragos T., 2020, *ApJL*, 895, L28
- Marchant P., Langer N., Podsiadlowski P., Tauris T. M., Moriya T. J., 2016, *A&A*, 588, A50
- Miller M. C., Hamilton D. P., 2002, *ApJ*, 576, 894
- Miller M. C., Lauburg V. M., 2009, *ApJ*, 692, 917
- Moe M., Di Stefano R., 2017, *ApJS*, 230, 15
- Muñoz D. J., Lai D., Liu B., 2016, *MNRAS*, 460, 1086
- Naoz S., 2016, *ARA&A*, 54, 441
- O’Leary R. M., Rasio F. A., Fregeau J. M., Ivanova N., O’Shaughnessy R., 2006, *ApJ*, 637, 937
- Olejak A., Fishbach M., Belczynski K., Holz D. E., Lasota J.-P., Miller M. C., Bulik T., 2020, *arXiv*, [arXiv:2004.11866](https://arxiv.org/abs/2004.11866)
- Özel F., Psaltis D., Narayan R., McClintock J. E., 2010, *ApJ*, 725, 1918
- Petrovich C., Antonini F., 2017, *ApJ*, 846, 146
- Pijloo J. T., Caputo D. P., Portegies Zwart S. F., 2012, *MNRAS*, 424, 2914
- Podsiadlowski P., Rappaport S., Han Z., 2003, *MNRAS*, 341, 385
- Portegies Zwart S. F., McMillan S. L. W., 2000, *ApJ*, 528, L17
- Randall L., Xianyu Z.-Z., 2018, *ApJ*, 853, 93
- Rauch K. P., Tremaine S., 1996, *NewA*, 1, 149
- Repetto S., Nelemans G., 2015, *MNRAS*, 453, 3341
- Rodriguez C. L., Morscher M., Pattabiraman B., Chatterjee S., Haster C.-J., Rasio F. A., 2015, *PhRvL*, 115, 051101
- Rodriguez C. L., Kremer K., Grudić M. Y., Hafen Z., Chatterjee S., Fragione G., Lamberts A., et al., 2020, *ApJL*, 896, L10
- Samsing J., MacLeod M., Ramirez-Ruiz E., 2014, *ApJ*, 784,



71

- Samsing J., D’Orazio D. J., 2018, MNRAS, 481, 5445
- Samsing J., Hotokezaka K., 2020, arXiv, arXiv:2006.09744
- Sana H., de Mink S. E., de Koter A., Langer N., Evans C. J., Gieles M., Gosset E., et al., 2012, Sci, 337, 444
- Silsbee K., Tremaine S., 2017, ApJ, 836, 39
- Thompson T. A., 2011, ApJ, 741, 82
- Tian H.-J., El-Badry K., Rix H.-W., Gould A., 2020, ApJS, 246, 4
- Venumadhav T., Zackay B., Roulet J., Dai L., Zaldarriaga M., 2020, PhRvD, 101, 083030
- Wen L., 2003, ApJ, 598, 419
- Woosley S. E., 2017, ApJ, 836, 244
- Yang Y., Gayathri V., Bartos I., Haiman Z., Safarzadeh M., Tagawa H., 2020, arXiv, arXiv:2007.04781
- Zackay B., Venumadhav T., Dai L., Roulet J., Zaldarriaga M., 2019, PhRvD, 100, 023007
- Zevin M., Spera M., Berry C. P. L., Kalogera V., 2020, arXiv, arXiv:2006.14573
- Ziosi B. M., Mapelli M., Branchesi M., Tormen G., 2014, MNRAS, 441, 3703